A multi-objective optimization and multi-attribute decision-making analysis for technical-thermodynamic-economic evaluation considering the rock damage on production performance of hot dry rock geothermal resources

Xu, Fuqiang; Song, Xianzhi; Li, Shuang; Shi, Yu; Song, Guofeng; Lv, Zehao; Yi, Junlin

DOI
10.1016/j.applthermaleng.2024.122350

Publication date
2024

Document Version
Final published version

Published in
Applied Thermal Engineering

Applied Thermal Engineering 241 (2024) 122350

Contents lists available at ScienceDirect

Applied Thermal Engineering

journal homepage: www.elsevier.com/locate/apthermeng

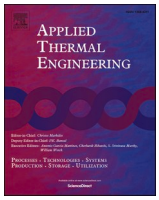

Research Paper

A multi-objective optimization and multi-attribute decision-making analysis for technical-thermodynamic-economic evaluation considering the rock damage on production performance of hot dry rock geothermal resources

Fuqiang Xu [a], Xianzhi Song [a], Shuang Li [a], Yu Shi [b,*], Guofeng Song [c], Zehao Lv [d], Junlin Yi [a]

[a] College of Petroleum Engineering, China University of Petroleum (Beijing), Beijing, China
[b] Faculty of Geosciences and Environmental Engineering, Southwest Jiaotong University, Chengdu, China
[c] Department of Geoscience and Engineering, Delft University of Technology, Delft, the Netherlands
[d] Petrochina Oil & Gas and New Energy Company, Petrochina Research Institute of Petroleum Exploration and Development, Beijing, China

ARTICLE INFO

Keywords:
Hot dry rocks
Damage
Production performance
Optimization
Decision-making
Multiple indicators

ABSTRACT

In the long-term mining of geothermal resources in hot dry rock (HDR), the change of thermal stress and pore pressure will increase fracture conductivity evolution, further improving production performance. The optimization and decision-making of the development scheme based on the impact of damage from fractures have yet to be reported. The damage to fractures is essential in designing and adjusting geothermal resource development schemes, particularly in selecting optimal schemes. Therefore, the production performances of HDR resources under different parameters are analyzed to establish a database. Then, minimizing flow resistance, maximizing net power, and maximizing economic benefits are set as optimization goals. Various injection-mining parameters and fracture characteristics are treated as decision variables. Multi-objective optimization and multi-attribute decision analysis is conducted to obtain optimal schemes. Finally, optimal schemes are evaluated and compared, considering damage and non-damage scenarios. Results show that the NSGA-II algorithm is more suitable for optimizing geothermal development questions. Net power and economic benefits of the optimal scheme considering damage increase by 45.84 % and 21.35 % compared to the control scheme with damage. For the non-damage scenario, the above values increased by 31.55 % and 5.15 %, respectively. Compared to not considering the damage, higher mass flow and well spacing of optimal scheme can be selected for the case when damaged. Moreover, the parametric design of the optimal scheme becomes more conservative as the production cycle increases.

1. Introduction

Hot dry rock is an essential part of medium-deep geothermal resources, which has the characteristics of high temperature, high pore pressure, dense lithology, etc [1]. Enhanced geothermal system (EGS) is the primary method for developing HDR resources. The implementation method is as follows [2]: firstly, a fracture network is manually created between injection wells and production wells; subsequently, cold fluid is pumped in for a heat exchange process, as shown in Fig. 1.

Fractures are the main channels for seepage and heat transfer in the reservoir for circulating working fluids [3]. In the long-term mining process, the fracture conductivity will change significantly due to the matrix elastic deformation and damage [4,5]. Previous studies have obtained the evolution characteristics of damage and its influence on production performance [6]. However, how do we integrate research on damage evolution into scheme design and adjustment optimization? Moreover, what is the difference between the optimal schemes with/without damage? The above questions still need to be solved.

In HDR resources mining, the evaluation of heat extraction performance contains multiple objectives coupled with many constraint variables [7]. Common optimization methods can be roughly divided into single-objective and multi-objective optimization [8]. Single-objective optimization occurs early and is suitable for simple engineering questions [9], which cannot comprehensively consider the diversity and

* Corresponding author.
E-mail address: shiyu@swjtu.edu.cn (Y. Shi).

https://doi.org/10.1016/j.applthermaleng.2024.122350
Received 11 June 2023; Received in revised form 19 November 2023; Accepted 2 January 2024
Available online 6 January 2024

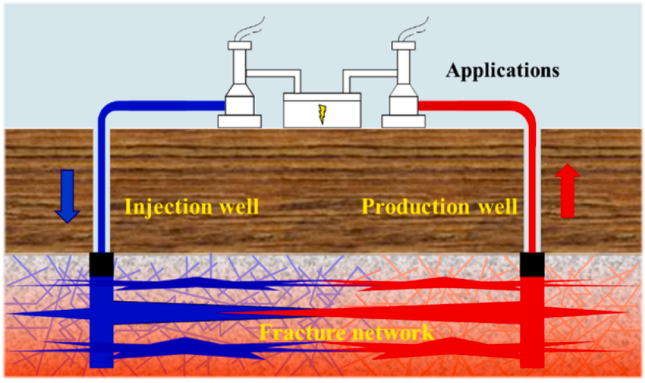

Fig. 1. Enhanced geothermal system schematic.

mutual exclusivity of the goals [7]. However, geothermal energy development is a typical multi-objective optimization question involving multiple goals, including economic, technical, and thermodynamic indicators. Multiple goals often conflict with each other, so a multi-objective optimization approach is typically employed to analyze and obtain a Pareto solution set [10,11].

For geothermal development and utilization, the existing multi-objective optimization is mainly carried out for the operation of organic Rankine cycle (ORC), geothermal well placement, borehole heat exchanger design, and multi-system joint application. For example, Liu et al. [12] used thermal efficiency, work output, exergy efficiency, and capital cost to evaluate the thermodynamic and economic performances of the ORC system. Wang et al. [13] assessed the performance of different types of ORC with maximizing exergy efficiency and minimizing cost of per net output power (PER) as the optimization goals, concluding that the basic ORC has the best performance with R245fa as the working fluid. Zhang et al. [14] optimized the well placement (well spacing) for geothermal wells in the Gonghe Basin, and the optimization goals included minimizing temperature drop and minimizing water level drawdown. Cruz-Peragón et al. [15] optimized the characteristics of the ground heat exchanger field (GHE), including disposition, number of boreholes, borehole depth, fluid temperature, etc., with maximizing energy savings and maximizing internal rate of return as the goal. Moreover, numerous economic-thermodynamic optimization studies have been carried out for the joint production of solar-geothermal energy [16–18].

The heat extraction process of HDR reservoirs involves coupling physical fields such as temperature, seepage, and stress fields [4]. It is subject to multiple constraints of reservoir physical properties, injection-mining parameters, and indication thresholds [7]. It is challenging to optimize and characterize goals such as power, flow resistance, economic benefits, etc. In the past, technical-thermodynamic optimization has been carried out, and the corresponding optimal scheme has been obtained [7,19]. However, the existing research has not considered the influence of damage evolution. The economic benefit is the key characteristic in the actual engineering development of HDR resources.

Moreover, the Pareto solution set obtained by optimization contains many optimization schemes [11], and combining subjective and objective data for comprehensive decision-making is necessary to get the optimal solution [20]. Multi-attribute decision-making refers to the identification of optimal schemes among several alternatives or the ranking of these options in order of merit. Several attributes express the schemes' advantages and disadvantages quantitatively or qualitatively [21]. Decision-making is often used in conjunction with optimization. It has been widely studied in the fields of energy [22,23], construction [24], and medicine [25], etc. However, the optimization and decision-making of production schemes under fracture damage are not

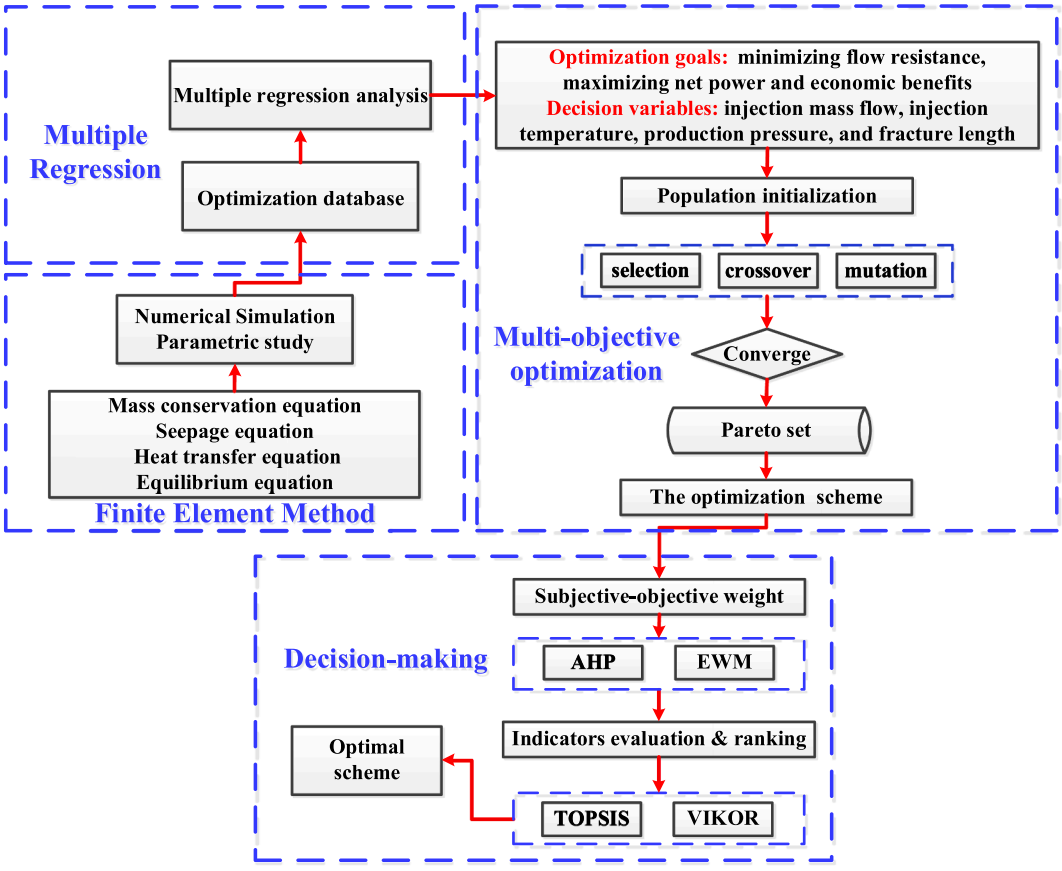

Fig. 2. Flow chart for the research.

considered for HDR mining. There are no relevant studies on the optimization algorithm selection, scheme evaluation, and effect comparison.

To obtain the optimal schemes, the current research is organized as follows: in section 2, the numerical model and the evolution characteristics of production performance are given; section 3 establishes the database and objective function and gives the process of algorithm selection and calculation; section 4 introduces the decision-making methods and optimal scheme acquisition process; in section 5, the influence of the production cycle on the optimal scheme is discussed; finally, section 6 summarizes the main conclusions. The flow chart for the research is shown in Fig. 2.

2. The model established and performance evaluation

2.1. Model assumptions and governing equations

The numerical model is the tool for parameter analysis, aiming to obtain the evolution law of production characteristics to form a database for optimization and decision-making. To facilitate the study, the following rationality assumptions are made: (1) except for Young's modulus and Poisson's ratio, other parameters of the rock are homogeneous and isotropic [26]; (2) during the mining process, the circulating fluid does not undergo phase change and satisfies Darcy's law, and its physical properties are detailed in the existing literature [4,27]; (3) working fluid does not react chemically with rocks; (4) heat transfer between fractures and rocks matrix satisfies the assumption of local non-thermal equilibrium [28]; (5) ignore water loss in the matrix during damage evolution.

The model-solving process involves the coupled calculation of the mass conservation, seepage, heat transfer, and equilibrium equations. The real-time transmission of multiple variables, such as pressure, velocity, temperature, damage variable, fracture aperture, and more facilitates the interaction among fluid flow, heat transfer, and stress evolution. Notably, damage evolution serves as a pivotal link.

Seepage equations in the rock matrix and fractures are as follows [29]:

$$\rho_f\left(\varphi_M C_f+\frac{1}{K_s}\left(1-\frac{K_d}{K_s}-\varphi_M\right)\right)\frac{\partial p}{\partial t}-\nabla\cdot\left(\rho_f\frac{k_M}{\mu_f}\left(\nabla p+\rho_f g\nabla z\right)\right) = -\rho_f\alpha_B\frac{\partial e}{\partial t}-Q_f \tag{1}$$

$$d_F\rho_f\left(\varphi_F C_f+\frac{1}{K_s}\left(1-\frac{K_d}{K_s}-\varphi_F\right)\right)\frac{\partial p}{\partial t}-\nabla_{\mathrm{T}}\cdot\left(d_F\rho_f\frac{k_F}{\mu_f}\left(\nabla_{\mathrm{T}}p+\rho_f g\nabla_{\mathrm{T}}z\right)\right) = -d_F\rho_f\alpha_B\frac{\partial e}{\partial t}+d_F Q_f \tag{2}$$

where ρ_f is the fluid density, kg/m^3; subscripts M and F represent the matrix and fracture, respectively; p is the pressure, Pa; t is the time, s; k is the permeability, m^2; μ_f is the fluid viscosity, Pa·s; g is the gravity acceleration, m/s^2; α_B is Biot-Willis coefficient; e is the volumetric strain; Q_f is the mass transfer between matrix and fractures, kg/(m^3·s); d_F is the fracture aperture, m; φ is the porosity; C_f is the fluid compressibility, Pa^{-1}; K_d is the drained bulk modulus of the porous matrix, Pa; K_s is the bulk modulus of a homogeneous block of the solid material, Pa.

The evolution expression of fracture conductivity under the action of matrix elastic deformation is as follows [30]:

$$k_F=\frac{d_h^2}{12}=\frac{\left(d_{h0}+\psi\Delta d_{F,n}\right)^2}{12} \tag{3}$$

where d_h and d_{h0} represent hydraulic aperture and initial hydraulic aperture, respectively, m; ψ is the coefficient for hydraulic aperture and geometric aperture transformation; $\Delta d_{f,n}$ is the normal deformation value of the geometric aperture, m.

Heat transfer in the matrix and fractures are given by the following expressions [28]:

$$\left((1-\varphi_M)\rho_s c_{p,s}+\varphi_M\rho_f c_{p,f}\right)\frac{\partial T_{\mathrm{M}}}{\partial t}-\rho_f c_{p,f}\nabla\cdot\left(\frac{k_M}{\mu_f}\left(\nabla p+\rho_f g\nabla z\right)\cdot T_M\right) -\nabla\cdot\left(\left((1-\varphi_{\mathrm{M}})\lambda_s+\varphi_M\lambda_f\right)\nabla T_M\right)=-Q_{f,E} \tag{4}$$

$$d_F\left((1-\varphi_F)\rho_s c_{p,s}+\varphi_F\rho_f c_{p,f}\right)\frac{\partial T_F}{\partial t}-d_F\rho_f c_{p,f}\nabla_{\mathrm{T}}\cdot\left(\frac{k_F}{\mu_f}\left(\nabla_{\mathrm{T}}p+\rho_f g\nabla_{\mathrm{T}}z\right)\cdot T_F\right) -\nabla_{\mathrm{T}}\cdot\left(\left((1-\varphi_F)\lambda_s+\varphi_F\lambda_f\right)d_F\nabla T_F\right)=d_F Q_{f,E} \tag{5}$$

where T_M is the rock matrix temperature, °C; ρ_s is the solid density, kg/m^3; $c_{p,f}$ and $c_{p,s}$ are the fluid and solid thermal capacity respectively, J/(kg·°C); T is the temperature, °C; λ_s and λ_f are the solid and fluid thermal conductivity respectively, W/(m·°C); $Q_{f,E}$ is the heat transfer between the reservoir matrix and fractures, W/m^3, which can be calculated from the product of the convective heat transfer coefficient and the fracture fluid-matrix temperature difference [31].

Under the influence of thermal stress and pore pressure changes, rock deformation can be characterized as [32]:

$$\frac{E}{2(1+\nu)}v_{i,jj}+\frac{E}{2(1+\nu)(1-2\nu)}v_{j,ji}-\alpha_B p\delta_{ij}-\frac{E}{1-2\nu}\alpha_T(T-T_0)+F_i=0 \tag{6}$$

where E is Young's modulus, Pa; ν is the Poisson's ratio; v is the displacement, m; δ_{ij} is the Cronek symbol; α_T is thermal expansion coefficient, 1/°C; T_0 is the reservoir initial temperature, °C; F_i is the body force per unit volume.

In this model, the tensile stress is positive, and compressive stress is negative. Maximum tensile stress criterion ($F_t \geq 0$) and the More-Coulomb criterion ($F_s \geq 0$) are used to determine whether the rocks are damaged [33]:

$$\begin{cases} F_t=\sigma_1-f_t=0 \\ F_s=-\sigma_3+\sigma_1\dfrac{1+\sin\varphi_f}{1-\sin\varphi_f}-f_c=0 \end{cases} \tag{7}$$

where f_t and f_c are the tensile and compressive strength, respectively, Pa; φ_f is the internal friction angle, ∘.

Previous experiments show that rock damage is dominated by tensile failure, so the maximum tensile stress criterion is analyzed first, and then the More-Coulomb criterion is analyzed [6]. Damage variables are characterized as follows [34]:

$$\omega=\begin{cases} 1-\left|\varepsilon_{t0}/\varepsilon_1\right|^n, & F_t\geqslant 0,\quad F_s<0 \\ 0, & F_t<0,\quad F_s<0 \\ 1-\left|\varepsilon_{c0}/\varepsilon_3\right|^n, & F_t<0,\quad F_s\geqslant 0 \end{cases} \tag{8}$$

where ω is a scalar damage variable, 0-undamaged, 1-completely damaged; ε_1 and ε_3 are major and minor principal strains respectively; ε_{t0} and ε_{c0} are the maximum tensile and compressive principal strain when tensile or/and shear damages occur, $\varepsilon_{t0}=f_t/E$, $\varepsilon_{c0}=-f_c/E$; n is a constitutive coefficient specified as 2.0 [35].

The evolution of physical properties characterizes the damage effect, and the relevant expressions are as follows [33,36]:

$$\begin{cases} E=(1-\omega)E_0 \\ f_c=(1-\omega)f_{c0} \end{cases},\quad \begin{cases} \varphi_m=\varphi_0+\left(\varphi_f-\varphi_0\right)\omega \\ k_m=k_{m0}\left(\dfrac{\varphi_m}{\varphi_0}\right)^3 e^{\beta\omega} \end{cases},\quad \lambda_s(T,\omega)=\lambda_{s0}e^{\omega/\delta_T} \tag{9}$$

where E_0 is Young's modulus without damage, Pa; f_c and f_{c0} are the compressive strength of the damaged and undamaged element,

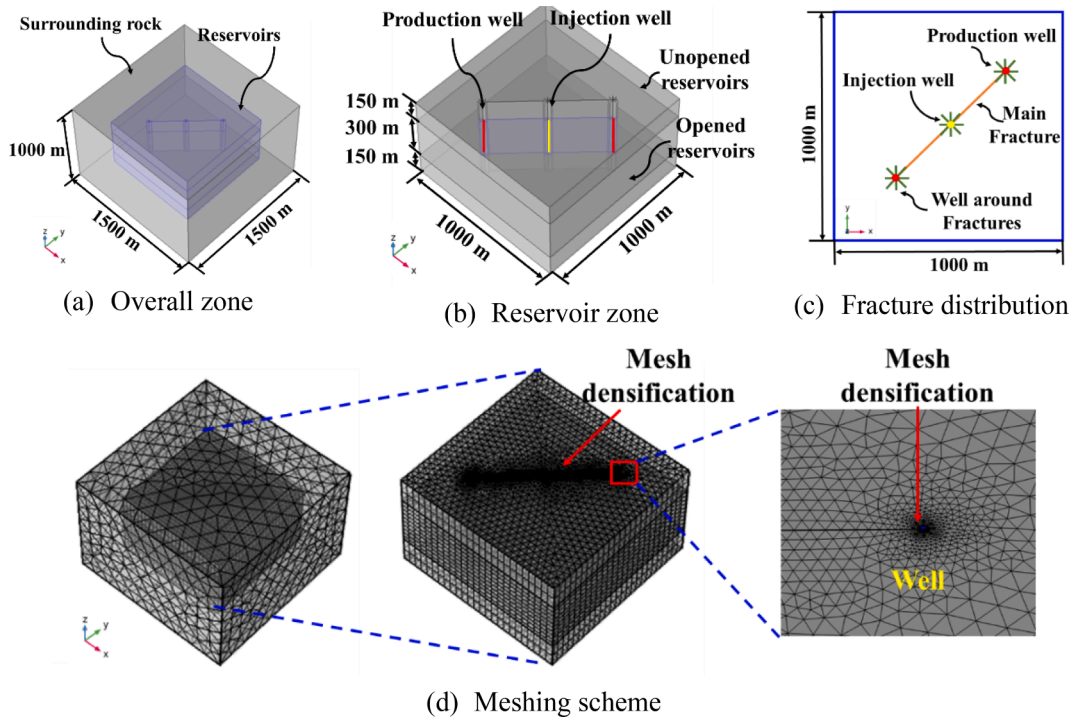

Fig. 3. Computational zone and meshing scheme.

Table 1
Parameter settings of the geometric model and conditions [38–40].

Items	Value	Items	Value
Zone size, km	1.5 × 1.5 × 1.0	Pressure at 3000 m, MPa	40
Depth ranges, km	3–4	Pressure gradient, Pa/m	5000
Reservoir size, km	1.0 × 1.0 × 0.6	Temperature at 3000 m, °C	250
Open layer thickness, m	300	Temperature gradient, °C /m	0.05
Unopen layer thickness, m	150	Injection rate, kg/s	50
Well spacing, m	350	Injection temperature, °C	50
Well diameter, m	0.10	Initial actual fracture aperture, m	3.8×10^{-4}
Well length, m	300	ψ coefficient	0.5
Half-length of well around fractures, m	10	Convective heat transfer coefficient, W/(m^2·°C)	3000
Production pressure, MPa	39.5	Internal friction angle, °	30

Table 2
Physical properties of the surrounding rock, reservoir, and fractures [40,41].

Items	Surrounding rock	Reservoir	Fracture
Density, kg/m^3	2800	2600	1200
Thermal conductivity, W/(m·°C)	3.0	2.9	2.0
Isobaric heat capacity, J/(kg·°C)	1000	950	800
Porosity	0.01	0.03	0.60
Initial permeability, m^2	10^{-18}	3.5×10^{-16}	3.5×10^{-11}
Thermal expansion coefficient, 1/°C	5×10^{-6}	5×10^{-6}	5×10^{-6}
Average Young's modulus, GPa	50	50	50
Tensile strength, MPa	10.5	10.5	10.5
Initial compressive strength, MPa	350	350	350
Average Poisson's ratio	0.25	0.25	0.25
Biot-Willis coefficient	0.7	0.7	0.7
Normal stiffness, GPa/m	/	/	80
Shear stiffness, GPa/m	/	/	50

respectively, Pa; φ_m, φ_0, and φ_f are the matrix porosity, initial matrix porosity, and fracture porosity, respectively; k_{m0} is the initial permeability of the matrix, m^2; β is damage-permeability effect coefficient; δ_T is damage-thermal conductivity effect coefficient.

Please refer to the available literature for a more detailed explanation of the equations and coupling relationships [37].

2.2. Geometric model and condition settings

The outside of the reservoir is surrounded by surrounding rock, and the model computational zone is a cube, as shown in Fig. 3(a). The reservoir is located in the center and divides into unopened and open reservoirs. An opened reservoir refers to the reservoir through perforation and other processes. Fracture is within the reservoir, divided into primary fractures (through injection and production wells) and fractures around the well. The model uses triangular prismatic elements (reservoir) and free tetrahedron elements (surrounding rock) for meshing, and the freedom degree reaches 2.16 million, as shown in Fig. 3(d). Parameter settings of the geometric model are detailed in Table 1 [38–40], and the physical properties of the surrounding rock, reservoir, and fractures are shown in Table 2 [40,41].

The injection well is located at the midpoint of the connection between the two production wells. The model adopts constant mass flow injection and constant pressure production. All model boundaries are set to no-flow and open temperature boundaries [29]; other parameter settings of initial and boundary conditions are shown in Table 1. Before the cold water is injected, the internal forces of the rock are balanced, and the triaxial stress is set to 68 MPa [40]. In previous studies, numerical models have been extensively validated [6,37]. The total period is ten years, and the time step is 0.5 d.

2.3. Performance evaluation indicators

This study defines flow resistance, net heat extraction power, and economic benefit as evaluation indicators, called technical-thermodynamic-economic indicators. Net heat extraction power (P_n, MW) represents the heating rate of the geothermal system and is

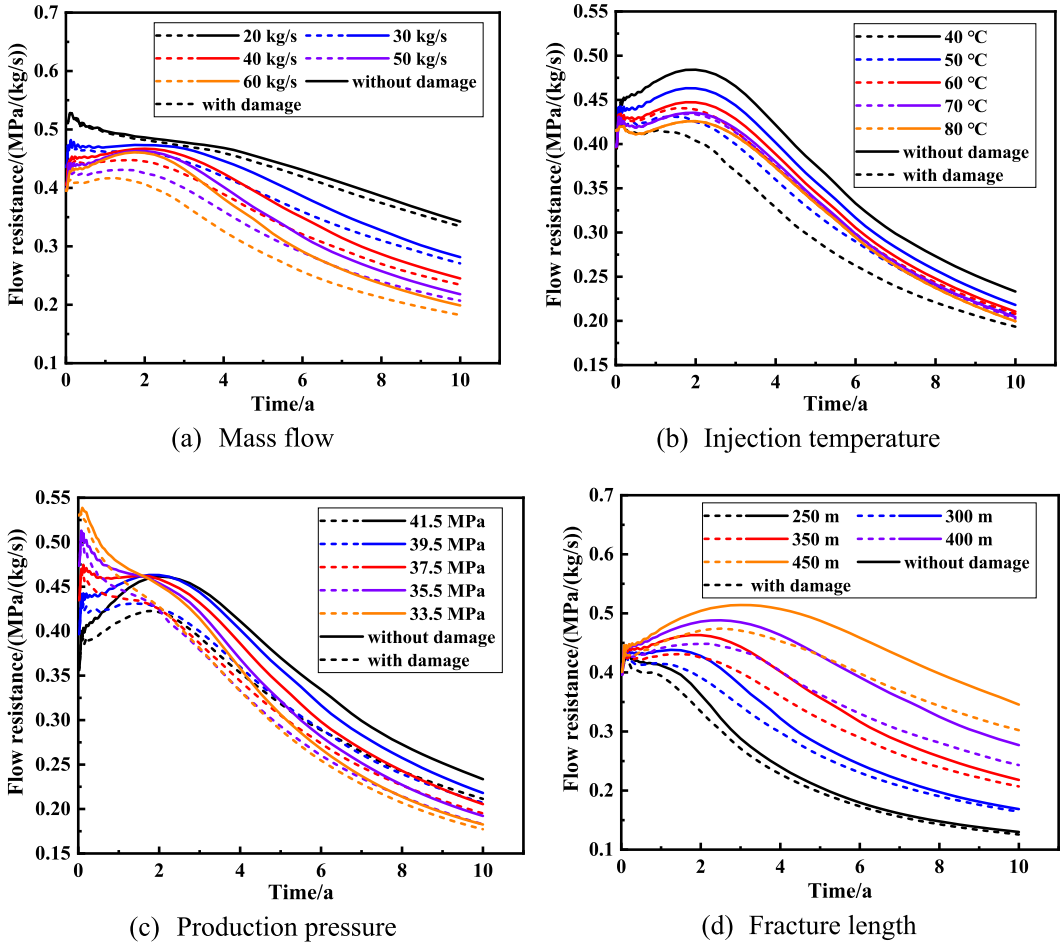

Fig. 4. Evolution of flow resistance under different parameters.

calculated as:

$$P_n = \mathrm{q}_{\mathrm{ave},v}\rho_f c_{p,f}(T_{out} - T_{in}) \tag{10}$$

where $q_{ave,v}$ is the volume flow, m^3/s; T_{out} and T_{in} are the production temperature and injection temperature of the fluid, respectively, °C, and the above temperature values are the temperature of the well bottom.

Flow resistance (R, MPa/(kg/s)) is the ratio of differential pressure to fluid mass flow, which indicates the artificial "energy" pre-unit production rate [42]. It represents the need for injection capacity and is defined as follows:

$$R = \frac{p_{in} - p_{out}}{\mathrm{q}_{\mathrm{ave},v}\rho_f} \tag{11}$$

where p_{out} and p_{in} are the production pressure and injection pressure of the fluid, MPa.

Economic benefit (E, RMB) includes the electrical energy consumption of the pump, heat sales revenue, and other costs, as follows [43,44]:

$$\begin{cases} E = -E_{\mathrm{pump}} + E_T - E_o \\ E_{\mathrm{pump}} = p_e \mathrm{q}_{ave,v}(p_{in} - p_{out})/\eta_p \\ E_T = p_T \eta_T \mathrm{q}_{ave,v}\rho_f c_{p,f}(T_{out} - T_{in}) \\ E_o = E_w + E_m + E_l \end{cases} \tag{12}$$

where E_{pump} is the cost of electricity, RMB; E_T is the benefits from heat sales, RMB; E_o is the other cost incurred due to tailwater treatment (E_w), post-maintenance (E_m), and labor services (E_l), RMB; p_e is the price of electrical power, 0.45 RMB/kW•h; η_p is the pump efficiency, 75.0 %; p_T is the price of heat application, 0.22 RMB/kW•h; η_T is the efficiency of geothermal power generation, 12.0 %.

2.4. Parameters effect

Taking the three indicators of section 2.3 as the evaluation object, the effects of injection mass flow, injection temperature, production pressure, and fracture length (well spacing) are analyzed.

Fig. 4 shows the evolution characteristics of flow resistance under different parameters. Under the action of all parameters, the overall trend of the flow resistance evolution curve decreases, and there is a slight rising segment. In the beginning, the increase in flow resistance is due to the increment in fluid viscosity as the temperature decreases. In the later stages, the continuous sloping portion is due to elastic deformation and damage, leading to increased fracture conductivity. The flow resistance value with damage is significantly smaller than without damage, and the above law applies to all the study parameters. In the 10th year, the maximum flow resistance differences under each parameter with or without damage are 0.016, 0.040, 0.022, and 0.043 MPa/(kg/s), respectively.

Moreover, the flow resistance is minor under high mass flow in the study setting. Although increasing the mass flow will lead to the growth in differential pressure, the flow resistance as a ratio, the growth of the numerator (differential pressure) in the corresponding fraction is less than that of the denominator (mass flow), so the flow resistance value decreases. The evolution curves for the consideration and without consideration of damage at 40 °C are located at the bottom and top of all curves, respectively. The former is because the damage at low temperatures significantly increases the permeability of the reservoir, while the latter is because of the high viscosity of the low-temperature fluid. Fluids are more accessible to extract at low production pressures, so the flow resistance is relatively small. However, the choice of production

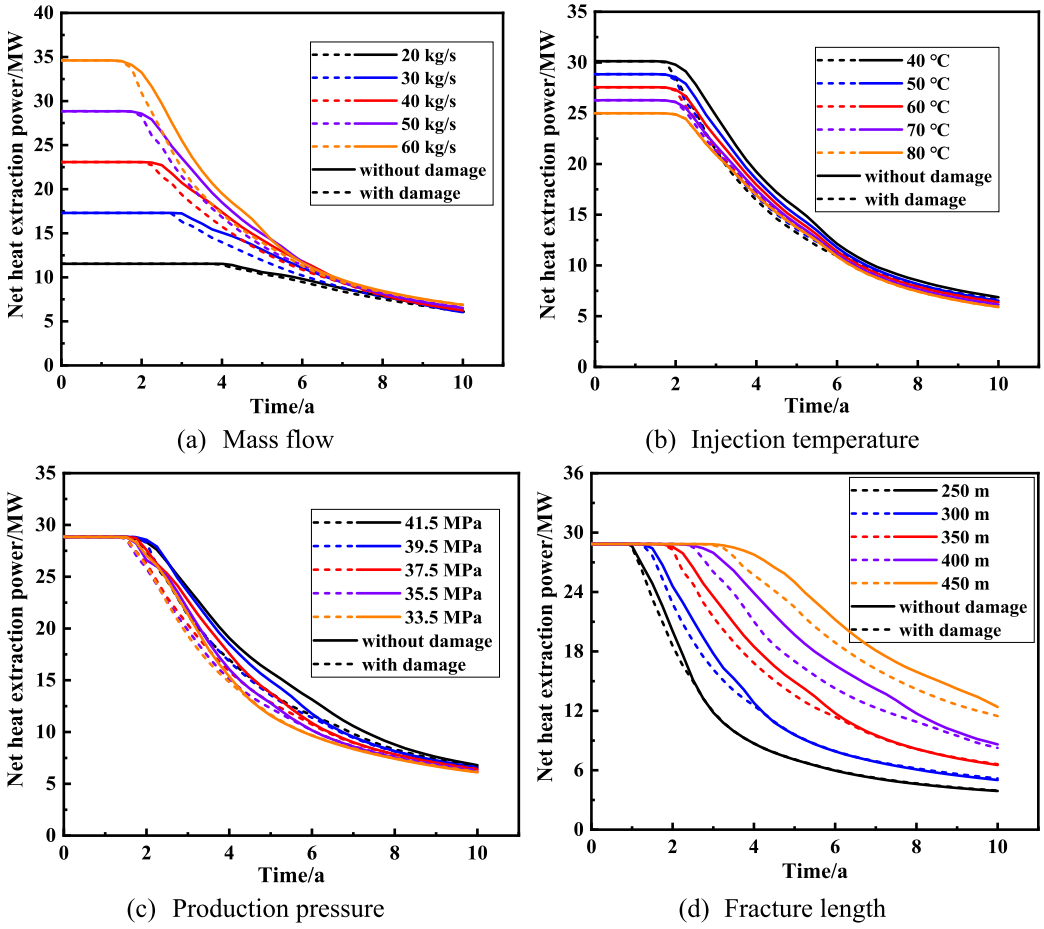

Fig. 5. Evolution of net heat extraction power per well under different parameters.

pressure is related to the power of the surface pump, and its selection needs to consider both cost and pump performance. Under the long fracture length, the seepage distance of the fluid increases, so the flow resistance is relatively large.

The evolution characteristics of net heat extraction power per well (from now on referred to as "net power" for simplicity) under different parameters are shown in Fig. 5. All curves remained flat and then fell rapidly, with turning points coinciding with the timing of the thermal breakthrough. Similarly, the net power value with damage is significantly smaller than without damage, and the power starts dropping slightly earlier. In the 10th year, except for the maximum differential net power of 0.921 MW under fracture length, the curves under the influence of other parameters are almost coincident, indicating a stable state.

The difference in net power at different mass flows is apparent at the initial moment. The net power increases with an increase in mass flow, and the maximum difference exceeds 20 MW. The difference gradually decreases in the later stage because the temperature drops rapidly despite the large amount of fluid at high mass flow, and according to Eq. (10), the product of mass flow and temperature gradually reaches a stable value. Moreover, the turning point moments (thermal breakout time) appear earlier as the mass flow increases. The effect of temperature on net power is similar to that of mass flow, but the difference in initial values is relatively small, around 5 MW. Moreover, initial net power is consistent under different production pressures and fracture lengths. Compared with other parameters, the influence of fracture length on net power evolution is the most significant. The longer fracture length delays the moment when the net power curve begins to decrease, and the turning point of each curve is about 1.0 a, 1.5 a, 2 a, and 2.5 a, respectively.

The evolution of economic benefit under different parameters is shown in Fig. 6. Each curve shows an upward and downward trend. As mentioned earlier, the expenditure items are mainly pump consumption, water treatment, and maintenance costs, and the revenue items are mainly heat sales. The root cause of the decline in economic benefit is that the production temperature is too low to reach breakeven and even negative values under some parameter settings, confirming the necessity for optimization.

Moreover, due to the comprehensive influence of many factors, there is no uniform law of economic benefit difference with/without damage. Under different production pressures, the economic benefits exhibit alternating positive and negative differences, as shown in Fig. 6(c). Compared with the case without consideration of damage, the economic benefit with damage decreases under lower injection flow and higher injection temperature. In other cases, the economic benefits increase after considering the damage.

From the above analysis, the effect of each parameter on indicators has a major and a secondary. To analyze the contribution of each parameter, the priority comparison results are obtained by taking the production characteristics in the 5th year as the object, as shown in Fig. 7. Among them, Fig. 7(a), (c), and (e) are the comparison results of indicators value considering the damage. Fig. 7(b), (d), and (f) are comparison results of indicators of difference value with/without damage. The data analysis method is the Grey Relation Analysis [13].

The fracture lengths have the most significant effect on each indicator, which are 0.831 (flow resistance), 0.833 (net power), and 0.780 (economic benefit), ranking first. The ranking is followed by production pressure, corresponding values of 0.776, 0.796, and 0.742, respectively. Injection mass flow is ranked behind the injection temperature, and the

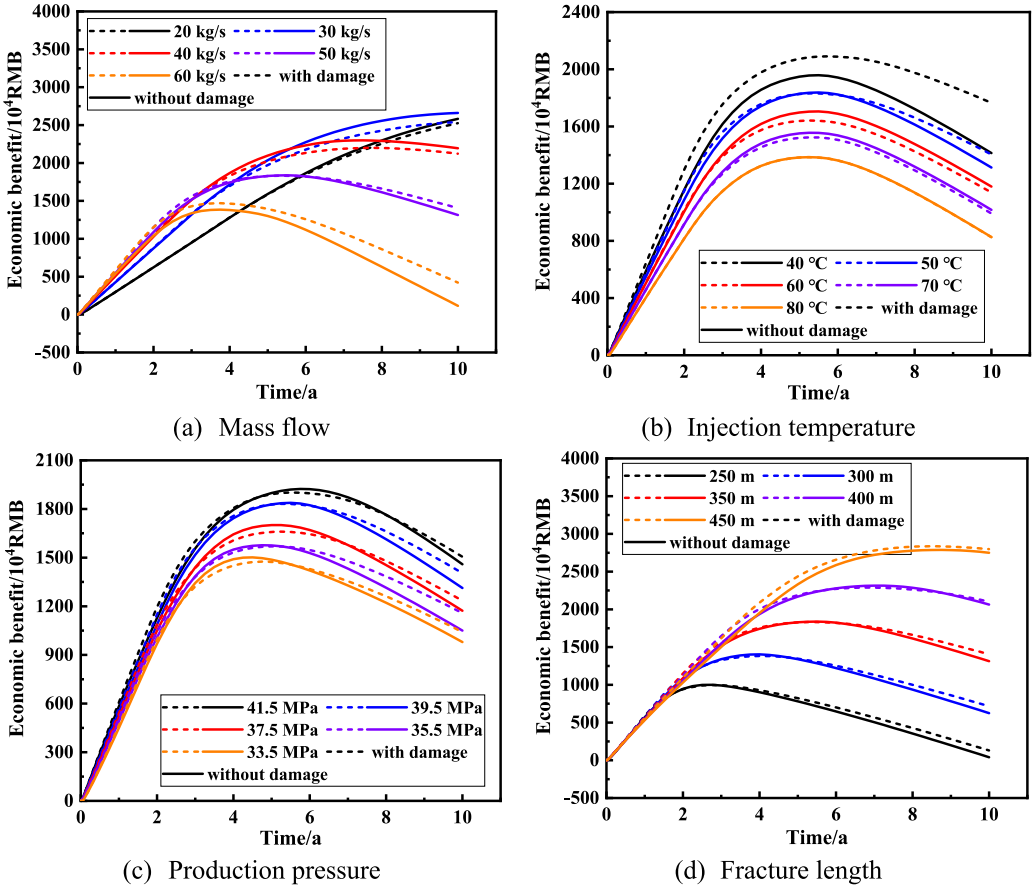

Fig. 6. Evolution of economic benefit under different parameters.

corresponding values are 0.641, 0.695, and 0.627, respectively. Unlike the actual effect reflected in the indicators value analysis results, the differential indicators analysis results reflect the impact of damage on production performance. Form Fig. 7(b), (d), and (f), the effect of fracture length on differential flow resistance and differential net power is the most significant, followed by mass flow. The ranking of mass flow takes precedence for the differential economic benefit. Compared with other parameters studied, the injection temperature ranked last, corresponding to correlations of 0.686, 0.626, and 0.744, respectively. The sensitivity analysis provides data support and reference for later optimization and decision-making, for example, selecting decision variables and determining the objective function.

3. Multi-objective optimization of production schemes

3.1. Database and objective function

Combined with the analysis results of section 2.4 and supplementing the cross-study of various parameters, more than 100 sets of data are obtained. Through screening, 70 groups of results (5th year) with/without damage are selected for establishing the optimization and decision-making database, as shown in Appendix A.

Optimization goals include minimizing flow resistance, maximizing net power, and maximizing economic benefit. Moreover, injection mass flow, injection temperature, production pressure, and fracture length (well spacing) are the decision variables. The multiple linear regression analysis is used to establish the relationship between each goal and the variables. The corresponding expressions considering damage are as follows:

$$\begin{cases} R = a_0 + a_1 Q_{in} + a_2 Q_{in}^2 + a_3 T_{in} + a_4 T_{in}^2 + a_5 p_{out} + a_6 p_{out}^2 + a_7 L + a_8 L^2 \\ P_n = b_0 + b_1 Q_{in} + b_2 Q_{in}^2 + b_3 T_{in} + b_4 T_{in}^2 + b_5 p_{out} + b_6 p_{out}^2 + b_7 L + b_8 L^2 \\ E = c_0 + c_1 Q_{in} + c_2 Q_{in}^2 + c_3 T_{in} + c_4 T_{in}^2 + c_5 p_{out} + c_6 p_{out}^2 + c_7 L + c_8 L^2 \end{cases} \quad (13)$$

where a_0, a_1 … a_8 are coefficients between flow resistance and variables; b_0, b_1 … b_8 are coefficients between net power and variables; c_0, c_1 … c_8 are coefficients between economic benefit and variables; L is the fracture length, m.

Similarly, the expressions for optimizing goals and variables without damage are as follows:

$$\begin{cases} R = A_0 + A_1 Q_{in} + A_2 Q_{in}^2 + A_3 T_{in} + A_4 T_{in}^2 + A_5 p_{out} + A_6 p_{out}^2 + A_7 L + A_8 L^2 \\ P_n = B_0 + B_1 Q_{in} + B_2 Q_{in}^2 + B_3 T_{in} + B_4 T_{in}^2 + B_5 p_{out} + B_6 p_{out}^2 + B_7 L + B_8 L^2 \\ E = C_0 + C_1 Q_{in} + C_2 Q_{in}^2 + C_3 T_{in} + C_4 T_{in}^2 + C_5 p_{out} + C_6 p_{out}^2 + C_7 L + C_8 L^2 \end{cases} \quad (14)$$

where A_i, B_i, and C_i are the coefficients of flow resistance, net power, and economic benefit with the variables, respectively. The coefficients in Eqs. (13)–(14) are shown in Appendix B.

Fig. 8 shows the comparison results of actual values and regression values. With consideration of damage, the average errors for flow resistance, net power, and economic benefit are 2.81 %, 5.05 %, and 2.54 %, respectively. Without consideration of damage, the corresponding is 2.34 %, 3.20 %, and 1.35 %, respectively. In summary, the objective functions obtained by regression have met the needs.

In the production process, the injection-mining parameters are not arbitrarily designed but are set according to the ground facilities and

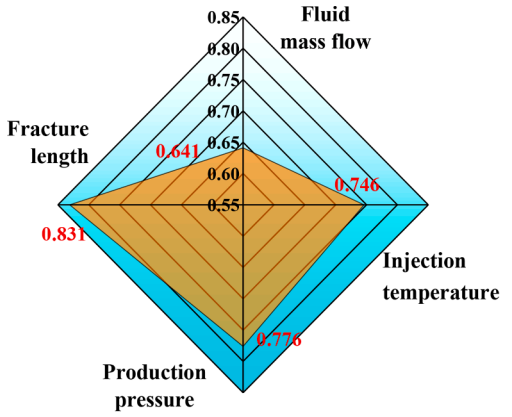

(a) Flow resistance, with damage

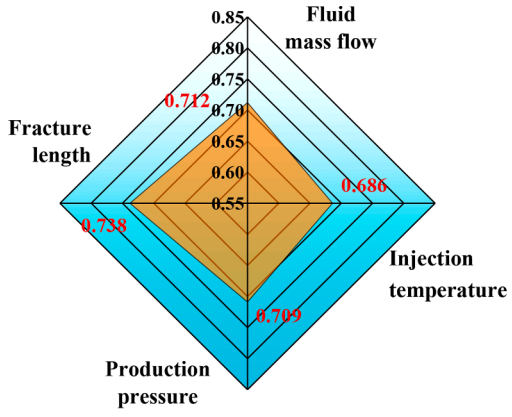

(b) Differential flow resistance with/without damage

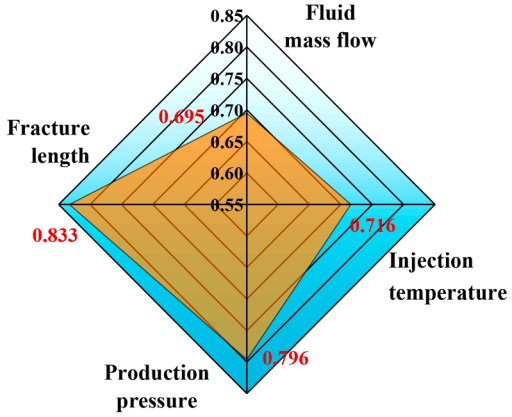

(c) Net power, with damage

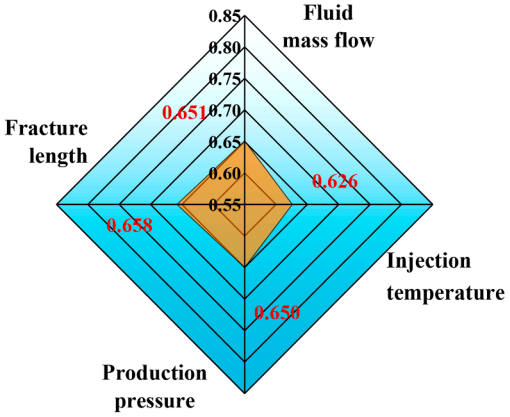

(d) Differential net power with/without damage

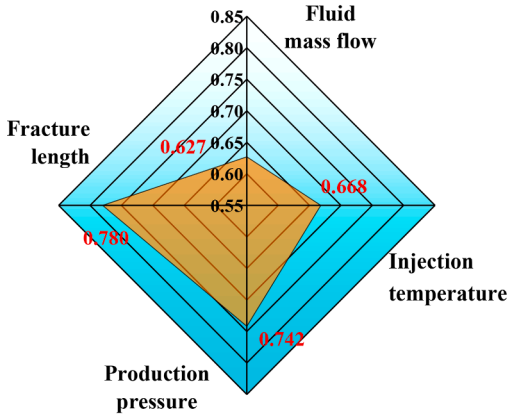

(e) Economic benefit, with damage

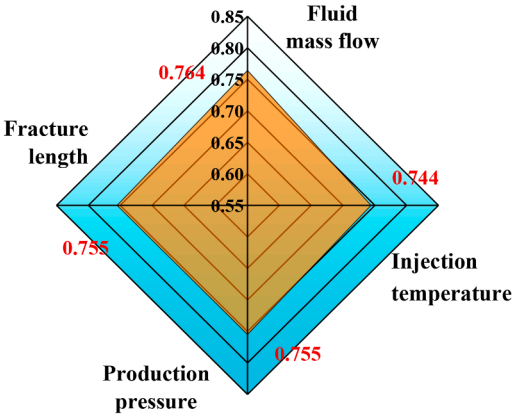

(f) Differential economic benefit with/without damage

Fig. 7. Parameter priority comparison of each indicator (5th year).

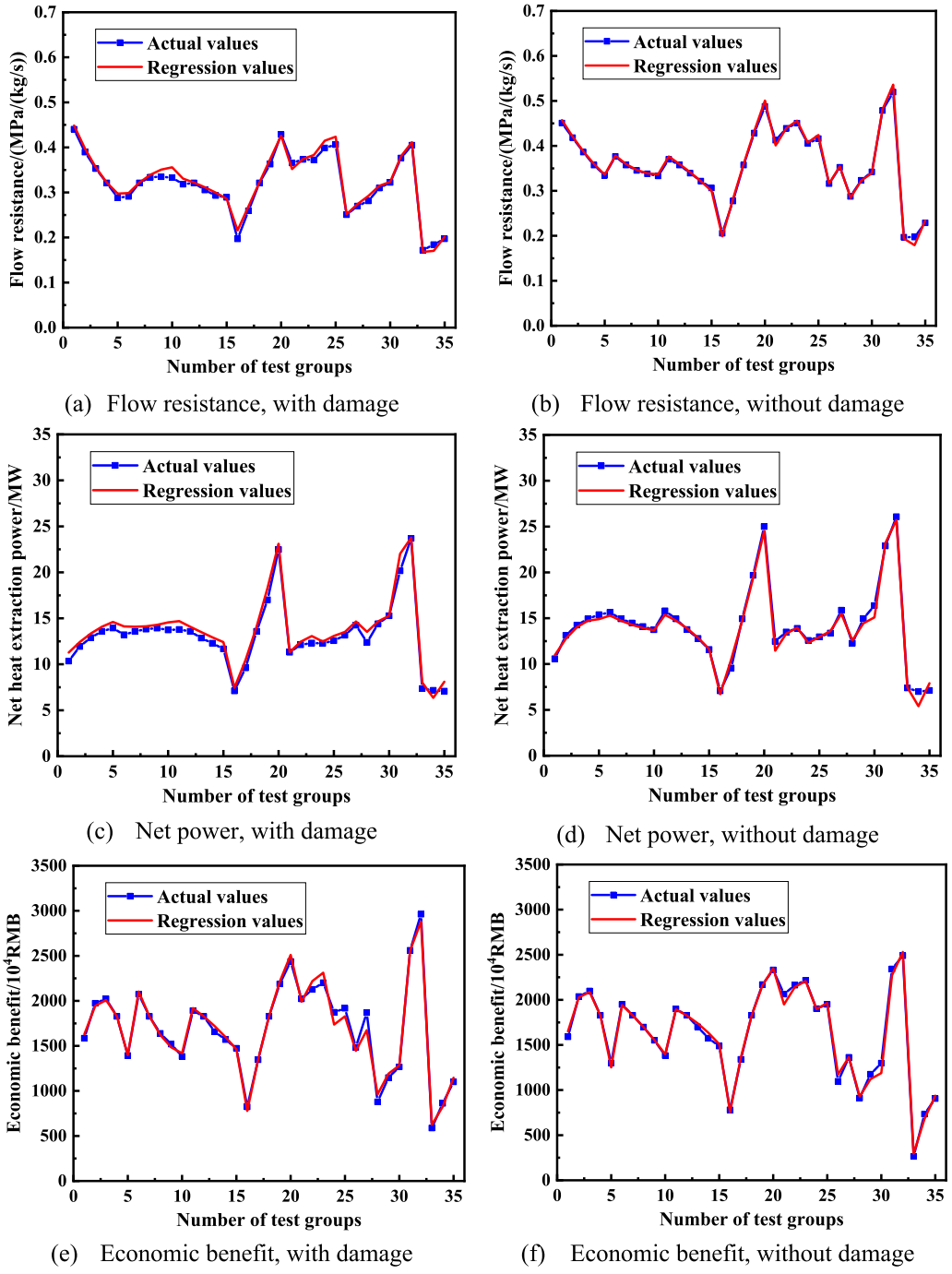

Fig. 8. Comparison results of actual and regression values (5th year).

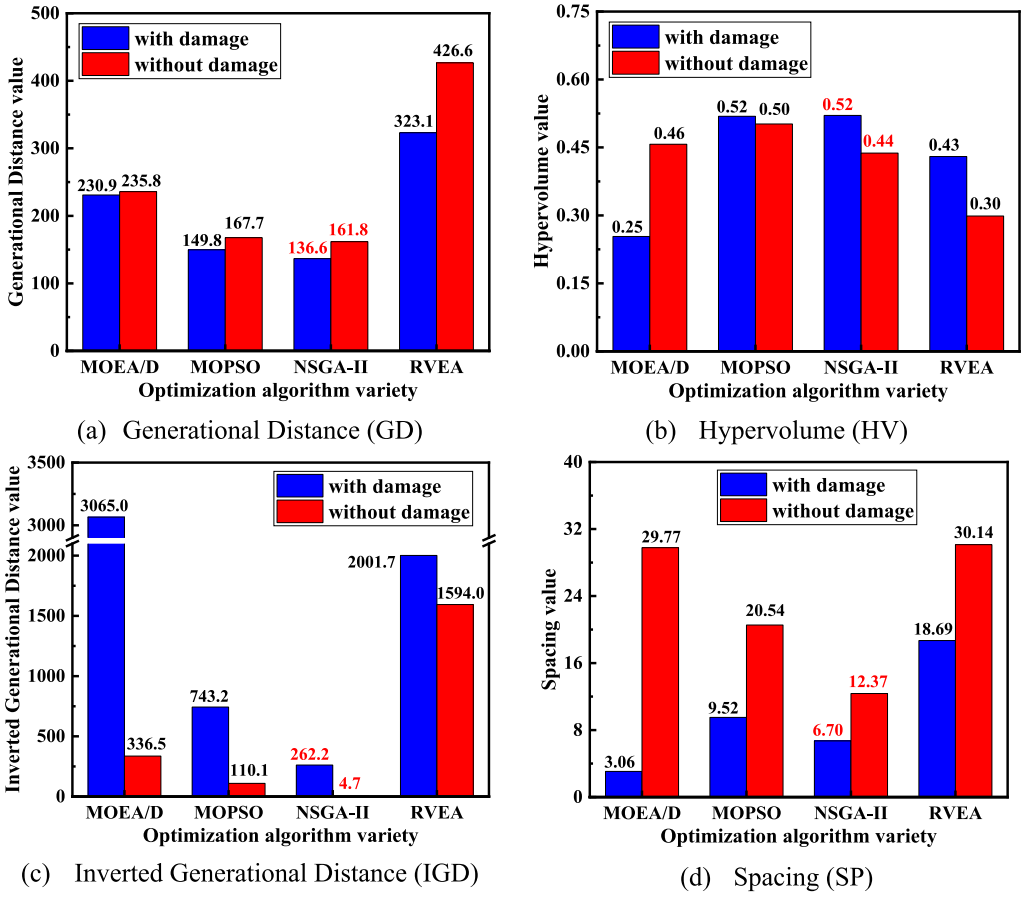

Fig. 9. Performance evaluation of different optimization algorithms (5th year).

actual needs, i.e., there are constraints. In this study, the main limitations include the bearing capacity of the surface pump, as well as the upper and lower limits of injection-mining parameters studied. Moreover, it is necessary to ensure that the values of each indicator are more significant than 0. Therefore, the constraints of this study are represented by the following equation:

$$\begin{aligned} &[\mathrm{x}]^T = [Q_{\mathrm{in}}\ T_{in}\ \mathrm{p}_{out}L]^T \\ &\min f(x) = (R(\mathrm{x}), -P_n(\mathrm{x}), -E(\mathrm{x})) \\ &s.t\begin{cases} [\mathrm{x}]^T = [Q_{\mathrm{in}}\ T_{in}\ \mathrm{p}_{out}L]^T \\ lb = [204033.5250]^T \\ ub = [608041.5450]^T \\ 42.5MPa \leqslant p_{in} \leqslant 60.0MPa \\ R > 0, \quad P_n > 0, \quad E > 0 \end{cases} \end{aligned} \tag{15}$$

Among them, the injection pressure-variable expressions with and without damage are shown in Eq.16, with average errors of 0.59 % and 0.90 %, respectively, which meet the analysis needs:

$$\begin{cases} p_{\mathrm{in,D}} = -38.631 + 0.374\mathrm{Q}_{\mathrm{in}} - 0.00209\mathrm{Q}_{\mathrm{in}}^2 + 0.240\mathrm{T}_{\mathrm{in}} - 0.00162\mathrm{T}_{\mathrm{in}}^2 \\ \qquad + 1.345\mathrm{p}_{out} - 0.00180\mathrm{p}_{out}^2 + 0.074L - 2.95 \times 10^{-5}L^2 \\ p_{\mathrm{in,W\text{-}D}} = -56.128 + 0.470\mathrm{Q}_{\mathrm{in}} - 0.00251\mathrm{Q}_{\mathrm{in}}^2 - 0.177\mathrm{T}_{\mathrm{in}} - 0.00106\mathrm{T}_{\mathrm{in}}^2 \\ \qquad + 2.148\mathrm{p}_{out} - 0.010\mathrm{p}_{out}^2 + 0.119L - 6.59 \times 10^{-5}L^2 \end{cases} \tag{16}$$

3.2. Algorithms selection

Multi-objective optimization solution is a research hotspot of various engineering, and different optimization algorithms have emerged. To select the algorithm suitable for this question, the comprehensive performances of some common algorithms are evaluated, such as Non-dominated sorting genetic algorithm II (NSGA-II) [45], Multi-objective evolutionary algorithm based on decomposition algorithm (MOEA/D) [46], Multi-objective particle swarm optimization algorithm (MOPSO) [47] and Reference vector guided evolutionary algorithm (RVEA) [48].

Performance evaluation indicators include Generational Distance (GD), Hypervolume (HV), Inverted Generational Distance (IGD), and Spacing (SP) [49], which are used to analyze the convergence, uniformity, and extensiveness of various algorithms in solving this question. Except for HV, smaller values for the other indicators indicate better algorithm applicability.

GD is the most classic convergence indicator, and it represents the average distance from the solution to the nearest reference point, where the reference set is uniformly sampled from the true Pareto frontier [50]:

$$GD(S,P) = \frac{\sqrt{\sum_{i=1}^{|S|} d_i^2}}{|S|} \tag{17}$$

where S is the solution set obtained by the algorithm; P is the Pareto approximation frontier; $d_i = \min_{p \in P} \left\| F(x^i) - F(p) \right\|, x^i \in S$, which calculates the Euclidean distance between x^i and the nearest reference point p on the Pareto approximation frontier.

HV measures the volume of the region in the target space enclosed by the undominated solution set obtained by the algorithm and the refer-

Table 3
Algorithm applicability ranking for each indicator.

Type	Method	GD	HV	IGD	IGD
With damage	MOEA/D	3	4	4	1
	MOPSO	2	1	2	3
	NSGA-II	1	1	1	2
	RVEA	4	3	3	4
Without damage	MOEA/D	3	2	3	3
	MOPSO	2	1	2	2
	NSGA-II	1	3	1	1
	RVEA	4	4	4	4

ence point, which can evaluate diversity (uniformity and extensiveness) and convergence [51]:

$$HV\left(S, z^{ref}\right) = volume\left(\bigcup_{i=1}^{|S|} c^i\right) \tag{18}$$

where c^i is the hypercube consisting of an undominated solution x and a reference point z^{ref} as diagonal.

IGD calculates the average distance from each reference point on the Pareto approximation frontier P to the closest solution in the solution set S. Similarly, it can measure both diversity and convergence [52]:

$$IGD(P,S) = \frac{\sqrt{\sum_{i=1}^{|P|} d_i^2}}{|P|} \tag{19}$$

where $d_i = \min_{x \in S} \left\| F(p^i) - F(x) \right\|, p^i \in P$, which calculates the Euclidean distance between the reference point p on the Pareto approximation frontier and the nearest solution x^i.

SP calculates the square of the difference between the two nearest solutions and their mean, which corresponds to the distribution of the solution set [53]:

$$SP(S) = \sqrt{\sum_{i=1}^{|S|} \frac{(d_i - \bar{d})^2}{|S| - 1}}, \quad \bar{d} = \frac{d_i}{|S| - 1} \tag{20}$$

where $d_i = \min_{x^j \in S, x^i \neq x^j} \left(\sum_{k=1}^{m} \left| F_k(x^i) - F_k(x^j) \right| \right)$, which is the Manhattan distance between x^i and x^j; $\bar{d}$ is the mean of d.

Fig. 9 shows the performance of each algorithm under different indicators. With consideration of damage, the values of each indicator of the NSGA-II algorithm are 136.6 (GD), 0.52 (HV), 262.2 (IGD), and 6.70 (SP), respectively, except for the SP indicator, which ranked second, and all other indicators are the first, as shown in Table 3. Without consideration of damage, the corresponding values of the NSGA-II algorithm

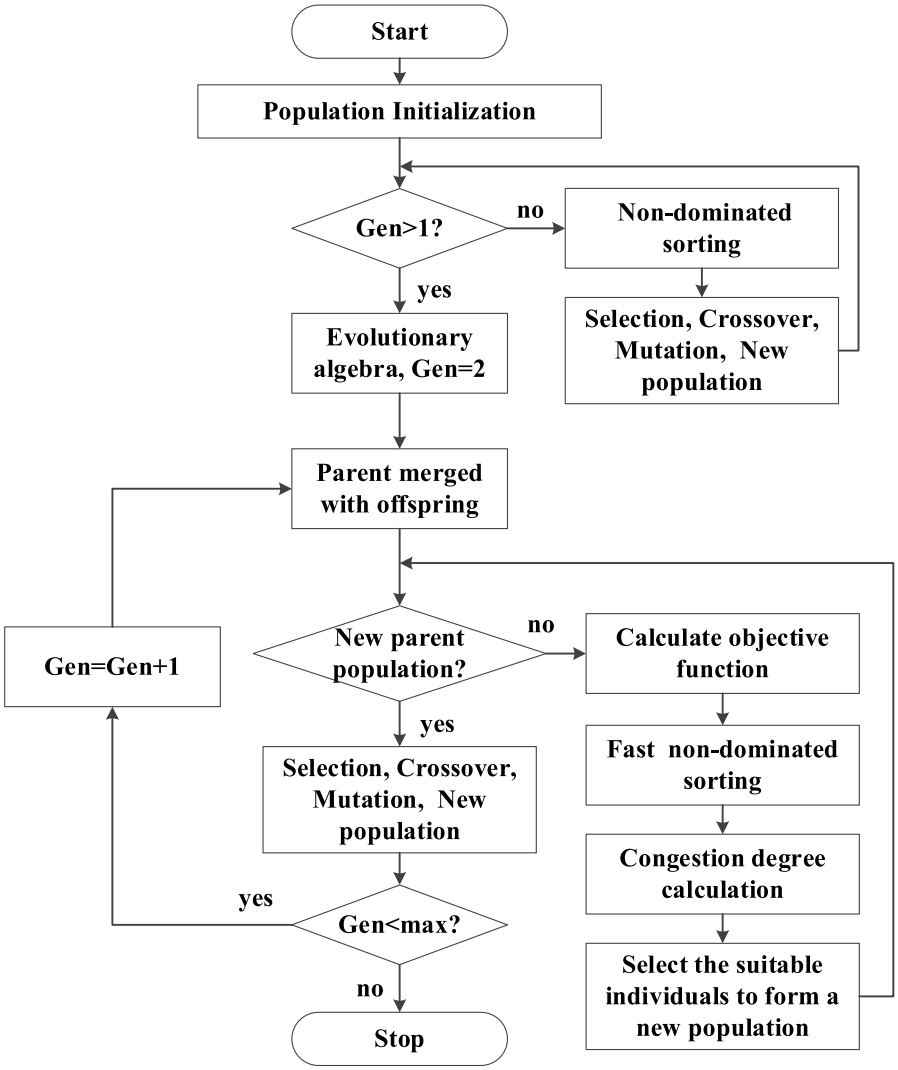

Fig. 10. The flow chart of the NSGA-II algorithm.

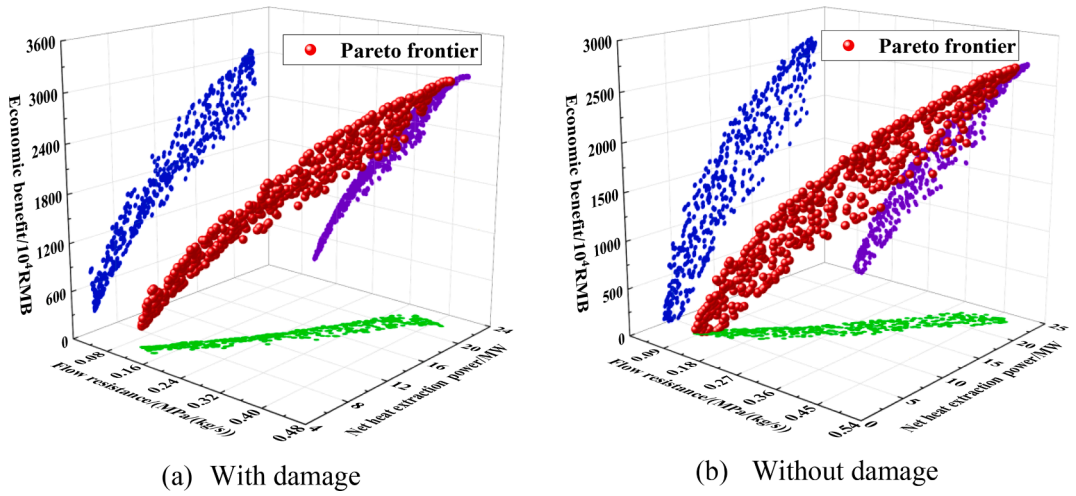

Fig. 11. Pareto solution sets with/without damage (5th year).

Table 4
Parameter settings and effect comparison of different optimization schemes (with damage).

Scheme	Items	Value	R,MPa/(kg/s)	P_n,MW	E, 10^4RMB
Scheme I	Q_{in}, kg/s	42.34	0.391	21.41	2979.67
	T_{in}, °C	40.00			
	p_{out}, MPa	41.04			
	L, m	441.88			
Scheme II	Q_{in}, kg/s	56.56	0.201	10.70	1415.51
	T_{in}, °C	40.02			
	p_{out}, MPa	40.16			
	L, m	301.24			
Scheme III	Q_{in}, kg/s	50.18	0.118	6.29	379.90
	T_{in}, °C	40.35			
	p_{out}, MPa	34.74			
	L, m	250.05			

are 161.8, 0.44, 4.7, and 12.37, respectively, except for the HV indicator, which ranks third, and all other indicators are the first, as shown in Table 3. Comprehensively analyzing various indicators, NSGA-II has better applicability to this question and is used for follow-up research.

NSGA-II is developed from the Genetic Algorithm (GA) combined with the Pareto concept [45]. The three advantages of NSGA-II are as follows [45]: (1) non-dominated sorting uses the concept of Pareto optimal solution to rank individuals in the population, which can select the better ones and give them a greater chance of moving on to the next iteration. Moreover, the complexity of the calculation is reduced; (2) comparing the superiority of individuals by congestion, and congestion degree operator is considered to ensure the diversity of the population; (3) elite strategy is to merge the current population with the subpopulation created by selection, crossing, and mutation, and jointly compete to produce the following population, ensuring that individuals with better characteristics can remain in the population, improving the diversity and computational efficiency of the population.

The flow chart of the algorithm is shown in Fig. 10, as follows [7]:

(1) Initialize the population and set the evolutionary algebra Gen = 1;
(2) Determine whether the first generation of the population has been generated, and if so, let the evolutionary algebra Gen = 2; otherwise, perform various operations on the initial population to generate the first generation of the population and make the evolutionary algebra Gen = 2;

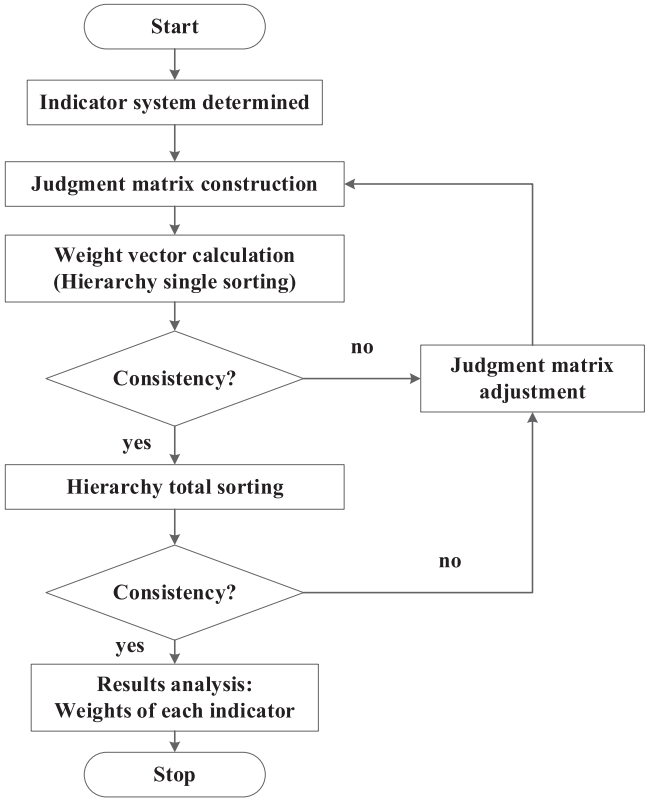

Fig. 12. The flow chart of the AHP method.

(3) Merging parent and offspring populations into new populations;
(4) Determine whether a new parent population has been generated. If not, calculate the objective function of the individual in the new population and perform various operations to generate a new parent population; otherwise, select, cross, and mutate the generated parent population to generate the offspring population;
(5) Determine whether Gen has reached the maximum evolutionary algebra. If not, add 1 to the evolutionary algebra and return to the third step; otherwise, the algorithm runs to the end.

Table 5
Weights of each indicator with/without damage (5th year).

Type	Method	Flow resistance	Net power	Economic benefits
With damage	AHP	59.36 %	24.93 %	15.71 %
	EWM	27.04 %	43.77 %	29.19 %
	Weighted	42.39 %	34.95 %	22.66 %
Without damage	AHP	59.36 %	24.93 %	15.71 %
	EWM	31.84 %	39.19 %	28.97 %
	Weighted	45.25 %	32.54 %	22.21 %

3.3. Acquisition of Pareto solution sets

Based on the objective function and process established above, the production schemes with or without damage are optimized and analyzed. The resulting Pareto solution sets are shown in Fig. 11. Among them, the red particles are the three-dimensional Pareto frontier. The other color particles are the projection of the Pareto frontier on each plane.

The number of populations set is 500. All schemes in the Pareto solution set can be considered alternative schemes, with no distinction between optimal and inferior. From Fig. 11, with consideration of damage, the change range of economic benefits, net power, and flow resistance is 2.62–30.64 million RMB, 5.75–22.43 MW, and 0.109–0.418 MPa/(kg/s), respectively. Without consideration of damage, the above changes range from 0.12 ten thousand RMB to 26.73 million RMB, 3.94 to 23.70 MW, 0.083 to 0.479 MPa/(kg/s). Regarding the upper and lower limits of the indicators corresponding to the optimization scheme, the above two situations have specific differences, which will be analyzed later.

Taking the situation under damage as an example, three different optimization schemes, I, II, and III, are randomly selected, as shown in Table 4. The economic benefits and net power corresponding to optimization scheme I are the highest, reaching 29.80 million RMB and 21.41 MW, respectively. However, the corresponding flow resistance is also the largest, reaching 0.391 MPa/(kg/s), indicating high demand for ground facilities. The flow resistance corresponding to the optimization scheme III is only 0.118 MPa/(kg/s), which is the lowest value among the three, but the economic benefit and net power are also the lowest, 3.80 million RMB and 6.29 MW, respectively, in terms of application alone, the heat extraction effect is poor. Optimization scheme II is a relatively balanced design solution, and the corresponding flow resistance, net power, and economic benefits are 0.201 MPa/(kg/s), 10.70 MW, and 14.16 million RMB, respectively.

In general, the above optimization scheme has no absolute advantages and disadvantages, but the focus on indicators (actual engineering requirements) is different. To obtain the optimal solution, it is necessary to carry out a decision-making analysis, which is exactly what section 4 is about.

4. Optimal schemes acquisition and comparison

4.1. Decision-making methods

The data source for optimization scheme decision-making is the Pareto solution sets in section 3.3, and the primary process includes the weight determination and the comprehensive evaluation ranking of each indicator. The subjective–objective weight combination method is used to calculate the weight value of each indicator, among which the subjective method is AHP (Analytic Hierarchy Process) [54] and the objective method is EWM (Entropy Weight Method) [55].

AHP combines quantitative and qualitative analysis to judge the relative importance of each indicator using the experience of decision-makers, and the main steps are shown in Fig. 12. In this question, the flow resistance corresponds to the mining difficulty, which is the basis for whether the project can be put into production; Net power corresponds to actual application and is the basis for whether the project can be put into use. Therefore, the importance of the three indicators in section 2.3 is ranked as flow resistance (R) > net power (P_n) > economic benefits (E), which are used as inputs for AHP analysis.

EWM is an objective weighting method that determines the objective weight according to the degree of indicator variation [55]. The smaller the degree of indicator variation, the less information content it reflects and the lower the weight. Information entropy is the expectation of information content. The calculation of the EWM first requires data standardization:

$$Y_{ij} = \frac{X_{ij} - \min(X_j)}{\max(X_j) - \min(X_j)}, i = 1, 2..., m; j = 1, 2..., n \tag{21}$$

where Y is the standardized data value; X is the original data value; m is the number of indicators; n is the number of schemes.

Next, calculate the ratio (p_{ij}) and information entropy (e_j) corresponding to each indicator in each scheme as follows:

$$p_{ij} = Y_{ij} \Big/ \sum_{i=1}^{n} Y_{ij}, i = 1, 2..., m; j = 1, 2..., n \tag{22}$$

$$e_j = -\frac{1}{\ln n} \sum_{i=1}^{n} p_{ij} \ln p_{ij}, i = 1, 2..., m; j = 1, 2..., n \tag{23}$$

Table 6
Parameter settings and effect comparison of different schemes (5th year).

Scheme	Type	Items	Value	R,MPa/(kg/s)	P_n,MW	E, 10^4RMB
Optimal scheme with TOPSIS- VIKOR	With damage(Scheme IV)	Q_{in}, kg/s	59.61	0.315	19.79	2217.78
		T_{in}, °C	40.16			
		p_{out}, MPa	40.08			
		L, m	417.07			
	Without damage (Scheme V)	Q_{in}, kg/s	52.71	0.359	19.64	1922.88
		T_{in}, °C	56.18			
		p_{out}, MPa	37.47			
		L, m	410.76			
Control scheme	With damage(Scheme VI)	Q_{in}, kg/s	50.00	0.321	13.57	1827.56
		T_{in}, °C	50.00			
		p_{out}, MPa	39.50			
		L, m	350.00			
	Without damage (Scheme VII)	Q_{in}, kg/s	50.00	0.357	14.93	1828.66
		T_{in}, °C	50.00			
		p_{out}, MPa	39.50			
		L, m	350.00			

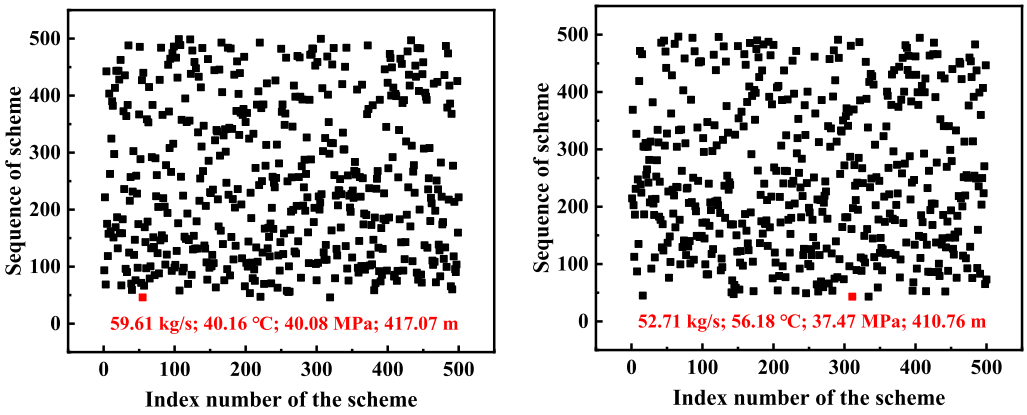

Fig. 13. Selection of the optimal scheme (5th year).

Finally, calculate the objective weights (β_j) of each indicator:

$$\beta_j = \frac{1-e_j}{\sum_{j=1}^{n}(1-e_j)}, j = 1, 2..., n \tag{24}$$

Subjective weights (α_j) obtained by AHP and the objective weights (β_j) obtained by EWM are recorded as the actual weights (ω_j) of the indicator:

$$\omega_j = \frac{\sqrt{\alpha_j \beta_j}}{\sum_{j=1}^{n}\sqrt{\alpha_j \beta_j}}, j = 1, 2..., n \tag{25}$$

The weights of each indicator calculated are shown in Table 5. There are differences in the weight distribution with/without damage using EWM. With consideration of damage, the weight of net power is the largest (43.77 %), and the flow resistance is the smallest, which is 27.04 %. Without consideration of damage, the weight of net power is also the largest (39.19 %), while the economic benefit is the smallest, at 28.97 %. After the subjective and objective weights are combined, the weight of flow resistance is the largest, reaching more than 40.00 %. The weights of net power and economic benefits are about 30.00 % and 20.00 %, respectively, and the weight difference of each indicator with/without damage is not apparent.

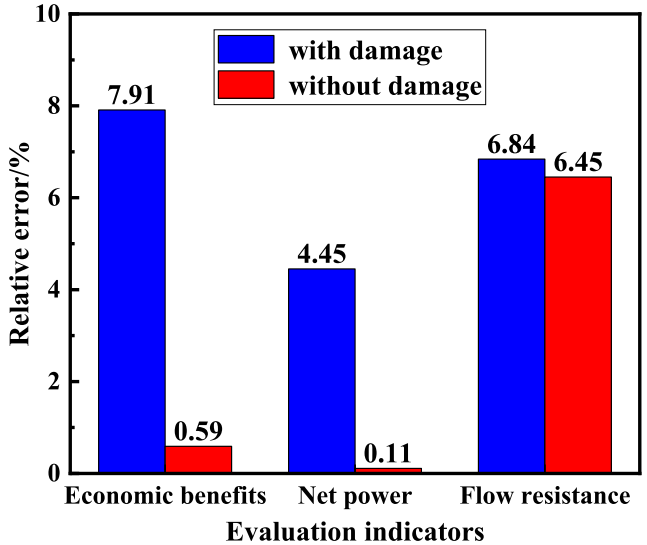

Fig. 14. Results comparison of the numerical solution and the optimized solution (5th year).

Next, the indicators are comprehensively evaluated and ranked. TOPSIS (Technique for order preference by similarity to ideal solution) [56] and VIKOR (VlseKriterijumska Optimizacija I Kompromisno Resenje) [57] are commonly used multi-objective decision-making methods.

In the TOPSIS, the positive and negative solutions to the evaluation problem are constructed. The schemes are sorted by calculating the relative proximity of each scheme to the ideal solution, that is, the degree close to the positive ideal solution and far from the negative ideal solution, and then the optimal solution is selected. The analysis steps of this method are divided into scheme processing, determination of positive and negative ideal solutions, Euclidean distance calculation, and comprehensive evaluation ranking [56].

First, the alternative schemes (Pareto solution set) are initialized, standardized, and weighted as follows:

$$V = \begin{vmatrix} x_{11} & x_{12} & \cdots & x_{1n} \\ x_{21} & x_{22} & \cdots & x_{2n} \\ \vdots & \vdots & \vdots & \vdots \\ x_{i1} & \cdots & x_{ij} & \cdots \\ \vdots & \vdots & \vdots & \vdots \\ x_{m1} & x_{m2} & \cdots & x_{mn} \end{vmatrix} \Rightarrow V' = \begin{vmatrix} x'_{11} & x'_{12} & \cdots & x'_{1n} \\ x'_{21} & x'_{22} & \cdots & x'_{2n} \\ \vdots & \vdots & \vdots & \vdots \\ x'_{i1} & \cdots & x'_{ij} & \cdots \\ \vdots & \vdots & \vdots & \vdots \\ x'_{m1} & x'_{m2} & \cdots & x'_{mn} \end{vmatrix} \Rightarrow U$$

$$= \begin{vmatrix} u'_{11} & u'_{12} & \cdots & u'_{1n} \\ u'_{21} & u'_{22} & \cdots & u'_{2n} \\ \vdots & \vdots & \vdots & \vdots \\ u'_{i1} & \cdots & u'_{ij} & \cdots \\ \vdots & \vdots & \vdots & \vdots \\ u'_{m1} & u'_{m2} & \cdots & u'_{mn} \end{vmatrix} \tag{26}$$

where V is the initialized scheme set, V' is the standardized scheme set, and U is the weighted scheme set.

Next, determine the positive and negative ideal solutions:

$$f_j^+ = \begin{cases} \max\left(x'_{ij}\right), j \in J^+ \\ \min\left(x'_{ij}\right), j \in J^- \end{cases}, i = 1, 2..., m; j = 1, 2..., n \tag{27}$$

$$f_j^- = \begin{cases} \min\left(x'_{ij}\right), j \in J^+ \\ \max\left(x'_{ij}\right), j \in J^- \end{cases}, i = 1, 2..., m; j = 1, 2..., n \tag{28}$$

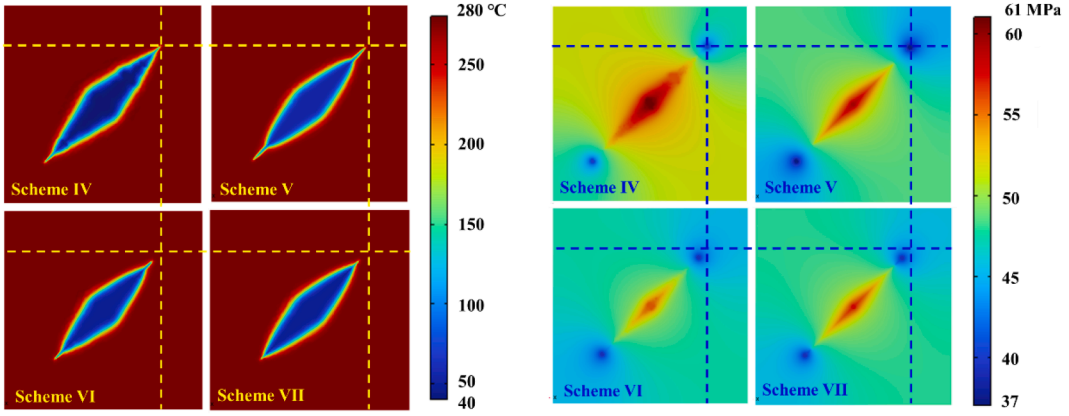

Fig. 15. Temperature field and pressure field characteristics of the different schemes (5th year).

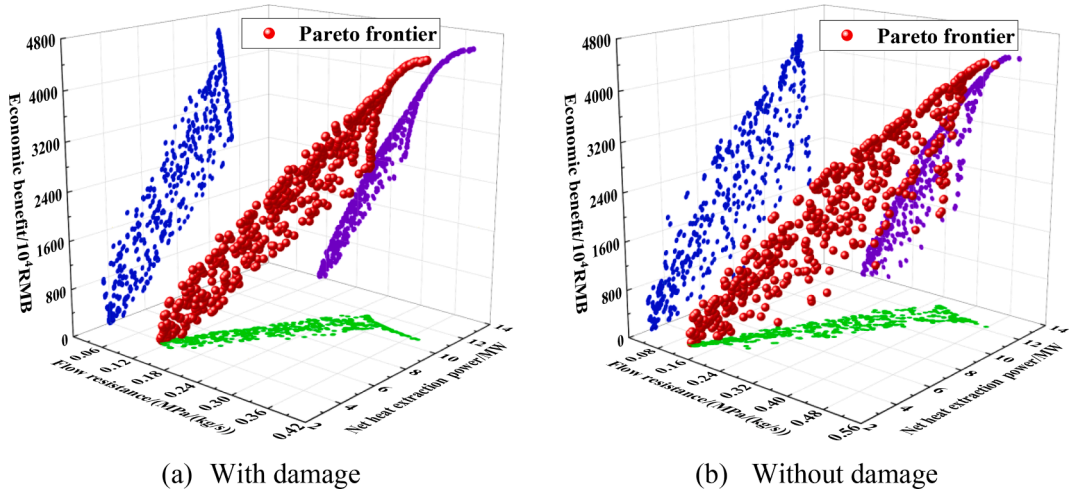

Fig. 16. Pareto solution sets with/without damage (10th year).

Table 7
Weights of each indicator with/without damage (10th year).

Type	Method	Flow resistance	Net power	Economic benefits
With damage	AHP	59.36 %	24.93 %	15.71 %
	EWM	21.94 %	37.54 %	40.52 %
	Weighted	39.27 %	33.28 %	27.45 %
Without damage	AHP	59.36 %	24.93 %	15.71 %
	EWM	21.10 %	39.13 %	39.77 %
	Weighted	38.63 %	34.09 %	27.28 %

where f_j^+ is the positive ideal solution and f_j^- is the negative ideal solution.

Then, calculate the Euclidean distance between scheme i and the ideal solution:

$$S_i^+ = \sqrt{\sum_{j=1}^{m}\left(x_{ij}^{'} - f_j^+\right)^2}, i = 1,2...,m; j = 1,2...,n \tag{29}$$

$$S_i^- = \sqrt{\sum_{j=1}^{m}\left(x_{ij}^{'} - f_j^-\right)^2}, i = 1,2...,m; j = 1,2...,n \tag{30}$$

where S_j^+ is the Euclidean distance between scheme i and the positive ideal solution, *and* S_j^- is the Euclidean distance between scheme i and the negative ideal solution.

Finally, the schemes are ranked according to the comprehensive evaluation indicator C, and the most significant C corresponds to the best scheme:

$$C = \frac{S_i^+}{S_i^+ + S_i^-}, i = 1,2,...,m \tag{31}$$

VIKOR is a compromise ranking method that compromises and ranks limited decision-making schemes by maximizing group utility and minimizing individual regret values [57]. Its main steps are as follows [57]:

First, standardize indicators:

$$x_{ij}^{'} = \frac{x_{ij} - \min\left(x_j\right)}{\max\left(x_j\right) - \min\left(x_j\right)}, i = 1,2...,m; j = 1,2...,n \tag{32}$$

Next, identify group utility (S_i) and individual regret (R_i):

$$S_i = \sum_{i=1}^{n} \omega_j \frac{\max\limits_{1\leqslant i\leqslant m} b_{ij} - b_{ij}}{\max\limits_{1\leqslant i\leqslant m} b_{ij} - \min\limits_{1\leqslant i\leqslant m} b_{ij}}, i = 1,2...,m; j = 1,2...,n \tag{33}$$

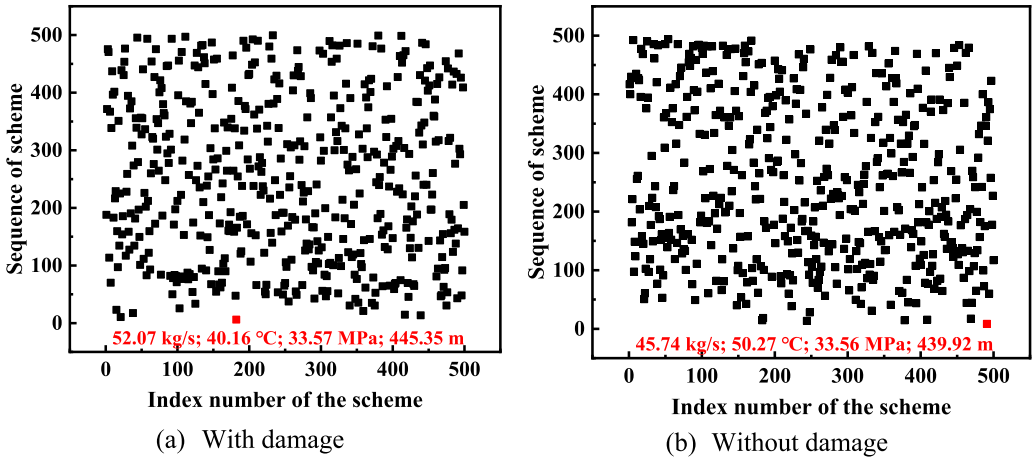

Fig. 17. Selection of the optimal scheme (10th year).

Table 8
Parameter settings and effect comparison of different schemes (10th year).

Scheme	Type	Items	Value	R,MPa/(kg/s)	P_n,MW	E, 10^4RMB
Optimal scheme with TOPSIS- VIKOR	With damage	Q_{in}, kg/s	52.07	0.240	10.31	2657.38
		T_{in}, °C	40.16			
		p_{out}, MPa	33.57			
		L, m	445.35			
	Without damage	Q_{in}, kg/s	45.74	0.305	10.85	2672.90
		T_{in}, °C	50.27			
		p_{out}, MPa	33.56			
		L, m	439.92			
Control scheme	With damage	Q_{in}, kg/s	50.00	0.207	6.61	1404.21
		T_{in}, °C	50.00			
		p_{out}, MPa	39.50			
		L, m	350.00			
	Without damage	Q_{in}, kg/s	50.00	0.218	6.53	1312.71
		T_{in}, °C	50.00			
		p_{out}, MPa	39.50			
		L, m	350.00			

$$R_i = \max_{1\leqslant j\leqslant n}\left[\omega_j \frac{\max_{1\leqslant i\leqslant m} b_{ij} - b_{ij}}{\max_{1\leqslant i\leqslant m} b_{ij} - \min_{1\leqslant i\leqslant m} b_{ij}}\right], i = 1,2...,m; j = 1,2...,n \tag{34}$$

Finally, according to the results of the group utility value and the individual regret value, the value of the decision-making indicator (Q_i) is calculated, and the smaller the indicator value, the better the scheme:

$$Q_i = \frac{0.5\left(S_i - \min_{1\leqslant i\leqslant m} S_i\right)}{\max_{1\leqslant i\leqslant m} S_i - \min_{1\leqslant i\leqslant m} S_i} + \frac{0.5\left(R_i - \min_{1\leqslant i\leqslant m} R_i\right)}{\max_{1\leqslant i\leqslant m} R_i - \min_{1\leqslant i\leqslant m} R_i}, i = 1,2...,m \tag{35}$$

4.2. Optimal schemes acquisition and comparison

Using the two methods described in section 4.1, an optimal scheme is obtained, and the results are shown in Table 6. Among them, the optimal scheme is determined by the minimum average of the sum of the TOPSIS and VIKOR schemes sorting, as follows:

$$N_{T-V} = \min \frac{N_{TOPSIS} + N_{VIKOR}}{2} \tag{36}$$

where N_{TV} is the final sequence number; N_{TOPSIS} is the sequence number with the TOPSIS method; N_{VIKOR} is the sequence number with the VIKOR method.

With consideration of damage, the injection mass flow, injection temperature, production pressure, and fracture length are 59.61 kg/s, 40.16 °C, 40.08 MPa, and 417.07 m, respectively, as shown in Fig. 13(a). Without damage, the above values are 52.71 kg/s, 56.18 °C, 37.47 MPa, and 410.76 m, respectively, as shown in Fig. 13(b). To verify the accuracy, the above parameters are substituted into the numerical model to compare the error of each indicator for the numerical solution and the optimized solution. As shown in Fig. 14, the maximum relative error between the two solutions is 7.91 %, and the average relative error is 4.39 %, which meets the requirements.

Fig. 15 illustrates the temperature and pressure field characteristics of the schemes presented in Table 6. Compared with the undamaged scenarios, the injection mass flow and fracture length (well spacing) of the optimal scheme considering damage are more significant, and the injection temperature is lower. The damage increases the fracture conductivity and reduces the difficulty of reservoir production, and a scheme requiring a larger differential pressure can be selected. During the study period (5th year), the temperature drops within an acceptable range, and lower fluid temperatures can be selected for maximum economic benefits. Correspondingly, there is no significant difference in net power with or without damage. The flow resistance of the former is reduced by 0.044 MPa/(kg/s), and the economic benefit is increased by 2.95 million RMB.

Compared with the control scheme, the injection mass flow and fracture length of the optimal scheme are increased, and the increases are 9.61 kg/s and 67.07 m with damage and 2.71 kg/s and 60.76 m

Table A1
Optimization and decision-making database.

	Q_{in}, kg/s	T_{in},°C	P_{out}, MPa	L, m	Flow resistance,MPa/(kg/s)		Net power,MW		Economic benefit,Million RMB	
					D	W-D	D	W-D	D	W-D
1	20	50	39.5	350	0.440	0.451	10.35	10.58	15.85	15.90
2	30	50	39.5	350	0.390	0.418	11.93	13.13	19.73	20.37
3	40	50	39.5	350	0.353	0.386	12.91	14.25	20.23	20.98
4	50	50	39.5	350	0.321	0.357	13.57	14.93	18.28	18.29
5	60	50	39.5	350	0.288	0.335	13.94	15.39	13.93	13.00
6	50	40	39.5	350	0.291	0.376	13.21	15.64	20.74	19.48
7	50	50	39.5	350	0.321	0.357	13.57	14.93	18.28	18.29
8	50	60	39.5	350	0.334	0.345	13.82	14.48	16.38	16.98
9	50	70	39.5	350	0.335	0.338	13.93	14.09	15.20	15.52
10	50	80	39.5	350	0.333	0.333	13.74	13.75	13.83	13.83
11	50	50	41.5	350	0.318	0.370	13.78	15.80	18.91	18.98
12	50	50	39.5	350	0.321	0.357	13.57	14.93	18.28	18.29
13	50	50	37.5	350	0.305	0.339	12.86	13.77	16.58	17.01
14	50	50	35.5	350	0.293	0.322	12.29	12.79	15.69	15.75
15	50	50	33.5	350	0.289	0.306	11.68	11.58	14.74	14.87
16	50	50	39.5	250	0.197	0.206	7.10	7.07	8.23	7.81
17	50	50	39.5	300	0.259	0.277	9.61	9.56	13.46	13.40
18	50	50	39.5	350	0.321	0.357	13.57	14.93	18.28	18.29
19	50	50	39.5	400	0.363	0.428	17.01	19.68	21.88	21.69
20	50	50	39.5	450	0.428	0.488	22.47	25.00	24.37	23.31
21	30	40	35.5	350	0.366	0.413	11.31	12.48	20.22	20.63
22	30	40	39.5	350	0.373	0.439	12.13	13.50	21.27	21.62
23	30	40	41.5	350	0.372	0.450	12.31	13.89	22.02	22.16
24	30	60	39.5	350	0.399	0.406	12.28	12.58	18.73	19.02
25	30	60	41.5	350	0.406	0.416	12.57	12.98	19.18	19.49
26	60	40	35.5	350	0.251	0.316	13.16	13.37	14.84	10.96
27	60	40	39.5	350	0.270	0.352	14.25	15.87	18.69	13.63
28	60	60	35.5	350	0.281	0.287	12.38	12.28	8.79	9.12
29	60	60	39.5	350	0.310	0.323	14.41	14.96	11.48	11.76
30	60	60	41.5	350	0.322	0.342	15.28	16.38	12.67	12.98
31	50	40	35.5	450	0.376	0.479	20.17	22.89	25.61	23.42
32	50	40	41.5	450	0.405	0.519	23.69	26.07	29.61	24.89
33	60	40	39.5	250	0.172	0.197	7.36	7.40	5.87	2.64
34	50	40	35.5	250	0.184	0.197	7.16	7.00	8.62	7.33
35	50	40	41.5	250	0.197	0.229	7.07	7.12	11.01	9.05

Table B1
The coefficient value and corresponding Significance *F*.

Factor	Value	Factor	Value	Factor	Value	Factor	Value
a_0	−0.481	b_7	-5.68×10^{-3}	A_0	−0.615	B_7	2.74×10^{-2}
a_1	-7.26×10^{-3}	b_8	1.16×10^{-4}	A_1	-4.84×10^{-3}	B_8	8.85×10^{-5}
a_2	4.43×10^{-5}	c_0	−7762.175	A_2	2.24×10^{-5}	C_0	-1.10×10^{4}
a_3	5.03×10^{-3}	c_1	93.384	A_3	-4.43×10^{-3}	C_1	117.051
a_4	-3.41×10^{-5}	c_2	−1.240	A_4	2.84×10^{-5}	C_2	−1.588
a_5	2.06×10^{-2}	c_3	−59.168	A_5	2.46×10^{-2}	C_3	−5.018
a_6	-2.17×10^{-4}	c_4	0.350	A_6	-2.24×10^{-4}	C_4	-7.17×10^{-2}
a_7	1.12×10^{-3}	c_5	194.531	A_7	2.21×10^{-3}	C_5	227.645
a_8	-1.06×10^{-7}	c_6	−1.830	A_8	-1.11×10^{-6}	C_6	−2.395
b_0	−9.439	c_7	21.471	B_0	−63.698	C_7	27.146
b_1	0.163	c_8	−0.018	B_1	0.314	C_8	-2.74×10^{-2}
b_2	-1.03×10^{-3}	*Significance F*		B_2	-2.66×10^{-3}	*Significance F*	
b_3	-5.05×10^{-2}	F_a	1.50×10^{-25}	B_3	−0.104	F_A	6.80×10^{-34}
b_4	5.14×10^{-4}	F_b	2.51×10^{-22}	B_4	5.27×10^{-4}	F_B	1.02×10^{-22}
b_5	2.51×10^{-2}	F_c	6.57×10^{-22}	B_5	2.312	F_C	2.25×10^{-26}
b_6	3.47×10^{-3}			B_6	-2.46×10^{-2}		

without damage, respectively. Correspondingly, the heat extraction performances are also greatly improved, and the optimal scheme's net power and economic benefits with damage are increased by 45.84 % and 21.35 %, respectively. At the same time, the flow resistance remains almost unchanged. Moreover, the net power and economic benefits of the optimal solution without damage are increased by 31.55 % and 5.15 %, respectively. The above studies show that through scheme optimization and decision-making, various indicators can be balanced to achieve reasonable and efficient development of HDRs.

5. Discussion

According to the above process, the optimization and decision-making research of the production scheme in the 10th year is carried out to analyze the impact of production time on the scheme design. The Pareto solution set is shown in Fig. 16. With consideration of damage, the change ranges of economic benefits, net power, and flow resistance are 1.06 ten thousand-45.04 million RMB, 3.70–11.54 MW, and 0.105–0.373 MPa/(kg/s), respectively. Without consideration of damage, the above changes range from 0.22 ten thousand RMB to 43.29 million RMB, 3.09 to 13.00 MW, and 0.108 to 0.477 MPa/(kg/s). Compared with the 5th year, the maximum net power in the 10th year is

significantly reduced, caused by the rapid decline in production temperature. Affected by this, the economic benefits have some values close to 0, or even negative value, but constraints limit it and are not reflected in the optimization scheme.

Table 7 shows the weight of each indicator in the 10th year, compared with the 5th year, the proportion of flow resistance has decreased, and the proportion of economic benefits has increased due to the following two points: (1) affected by the matrix elastic deformation and damage, the flow resistance decreased significantly, and the difference between parameters decreased; (2) changes ranges in economic benefits in the 10th year has increased significantly, with a maximum span of more than 45 million RMB, that is, the difference between parameters has increased. The above changes mean that the importance of economic benefit analysis in the scheme design with longer production cycles has increased.

Compared with the optimal scheme in the 5th year, the optimal scheme in the 10th year is more conservative in parameter design, reflected in the decrease in injection mass flow and the increase in fracture length, as shown in Fig. 17 and Table 8. Compared with the control scheme, the economic benefits of the optimal scheme are greatly improved, and the changes with/without damage are 89.24 % and 103.32 %, respectively, much greater than the improvement in the 5th year. The above phenomenon shows that time point is essential for scheme design.

6. Conclusion

To obtain the optimal scheme with damage evolution and economic evaluation in HDR mining, the law of parameter influence, multi-objective optimization, and multi-attribute decision-making analysis are carried out, and the conclusions are mainly as follows:

(1) For indicator value, the fracture lengths have the most significant effect, followed by production pressure, and mass flow is ranked behind the temperature. For indicators difference (with/without consideration of damage), the effect of mass flow has improved, especially the impact on economic benefits ranks first.
(2) The NSGA-II algorithm is more suitable for the multi-objective optimization analysis of this question. Comparing the Pareto solution set with/without damage, there are specific differences between them, which proves the necessity of optimizing and decision-making considering damage.
(3) Compared with the control scheme, the mass flow and fracture length of the optimal scheme increase by 9.61 kg/s and 67.07 m with damage, and 2.71 kg/s and 60.76 m without damage. Correspondingly, net power and economic benefits increase by 45.84 % and 21.35 % with damage and 31.55 % and 5.15 % without damage, while the difference in flow resistance is not apparent. Compared to not considering damage, the optimal scheme with damage corresponds to more significant mass flow and well spacing due to small flow resistance.
(4) The weights are sorted from most significant to most minor: flow resistance, net power, and economic benefit. Under the longer cycle, the weight of economic benefit increases, and the weight of flow resistance decreases, but the rank remains unchanged. Moreover, compared with the scheme in the 5th year, the scheme in the 10th year corresponds to a smaller mass flow and larger well spacing, i.e., it is more “conservative”.

CRediT authorship contribution statement

Fuqiang Xu: Data curation, Methodology, Software, Writing – original draft. **Xianzhi Song:** Conceptualization, Resources, Writing – review & editing, Project administration. **Shuang Li:** Formal analysis, Software, Validation, Writing – original draft. **Yu Shi:** Investigation, Resources, Writing – review & editing, Funding acquisition. **Guofeng Song:** Software, Supervision, Visualization. **Zehao Lv:** Data curation, Writing – original draft. **Junlin Yi:** Formal analysis, Writing – original draft.

Declaration of Competing Interest

The authors declare that they have no known competing financial interests or personal relationships that could have appeared to influence the work reported in this paper.

Data availability

Data will be made available on request.

Acknowledgments

The authors would like to acknowledge the National Natural Science Foundation of China (Grant No. 52104034, 52374010), the Major Program of the National Natural Science Foundation of China (Grant No. 52192624), the New Interdisciplinary Discipline Cultivation Fund of Southwest Jiaotong University (Grant No. 2682023ZTPY030, 2682022KJ034), the China Scholarship Council (Grant No. 202206440098).

Appendix A

The optimization and decision-making database is shown in Table A1. Among them, “D” is the condition considering the damage, and “W-D” is the condition without damage. Moreover, the database includes four duplicate studies to improve regression stability, with serial numbers 4, 7, 12, and 18.

Appendix B

The coefficients in Eqs. (13)–(14) are shown in Table B1. Among them, significance F refers to the p-value (probability), which reflects the probability of occurrence of an event. According to the P value obtained by the significance test method, $P < 0.05$ is generally considered a statistical difference. All significance F is less than 10^{-20}; both meet the requirements.

References

[1] J. Vidal, A. Genter, Overview of naturally permeable fractured reservoirs in the central and southern upper Rhine Graben: insights from geothermal wells, Geothermics 74 (2018) 57–73.
[2] Y. Shi, X.Z. Song, J.C. Li, G.S. Wang, F.X. YuLong, L.D. Geng, Analysis for effects of complex fracture network geometries on heat extraction efficiency of a multilateral-well enhanced geothermal system, Appl. Therm. Eng. 159 (2019) 113828.
[3] G.J. Yu, C. Liu, L.Z. Zhang, L.C. Fang, Parameter sensitivity and economic analyses of an interchange-fracture enhanced geothermal system, Adv. Geo-Energy Res. 5 (2) (2021) 166–180.
[4] G.F. Song, X.Z. Song, F.Q. Xu, G.S. Li, Y. Shi, J.Y. Ji, Contributions of thermo-poroelastic and chemical effects to the production of enhanced geothermal system based on thermo-hydro-mechanical-chemical modeling, J. Clean Prod. 377 (2022) 134471.
[5] T.K. Guo, Y.L. Zhang, W. Zhang, B.L. Niu, J.Y. He, M. Chen, Y. Yu, B. Xiao, R.L. Xu, Numerical simulation of geothermal energy productivity considering permeability evolution in various fractures, Appl. Therm. Eng. 201 (2022) 117756.
[6] F.Q. Xu, Y. Shi, X.Z. Song, G.S. Li, Z.H. Song, S. Li, The characteristics and laws of fracture damage in the long-term production process of high-temperature geothermal resources, Rock Mech Rock Eng 56 (2023) 275–299.
[7] G.F. Song, X.Z. Song, G.S. Li, Y. Shi, G.S. Wang, J.Y. Ji, F.Q. Xu, Z.H. Song, An integrated multi-objective optimization method to improve the performance of multilateral-well geothermal system, Renew Energ. 172 (2021) 1233–1249.
[8] G.F. Song, G.S. Li, X.Z. Song, Y. Shi, Multi-objective balanced method of optimizing the heat extraction performance for hot dry rock, Nat. Gas Ind. B 9 (2022) 497–510.
[9] Y.K. Zhou, S.Q. Zheng, G.Q. Zhan, A state-of-the-art-review on phase change materials integrated cooling systems for deterministic parametrical analysis, stochastic uncertainty-based design, single and multi-objective optimisations with machine learning applications, Energy Build. 220 (2020) 110013.

[10] F.Q. Xu, X.Z. Song, G.F. Song, J.Y. Ji, Z.H. Song, Y. Shi, Z.H. Lv, Numerical studies on heat extraction evaluation and multi-objective optimization of abandoned oil well patterns in intermittent operation mode, Energy 269 (2023) 126777.
[11] R.Y. Yang, Y.Y. Wang, G.F. Song, Y. Shi, Fracturing and thermal extraction optimization methods in enhanced geothermal systems, Adv. Geo-Energy Res. 9 (2) (2023) 136–140.
[12] X.M. Liu, M. Wei, L.N. Yang, X. Wang, Thermo-economic analysis and optimization selection of ORC system configurations for low temperature binary-cycle geothermal plant, Appl. Therm. Eng. 125 (2017) 153–164.
[13] Y.Z. Wang, J. Zhao, Y. Wang, Q.S. An, Multi-objective optimization and grey relational analysis on configurations of organic Rankine cycle, Appl. Therm. Eng. 114 (2017) 1355–1363.
[14] S.Y. Zhang, Z.J. Jiang, S.S. Zhang, Q.X. Zhang, G.H. Feng, Well placement optimization for large-scale geothermal energy exploitation considering nature hydro-thermal processes in the Gonghe Basin, China, J. Clean Prod. 317 (2021) 128391.
[15] F. Cruz-Peragón, F.J. Gómez-de la Cruz, J.M. Palomar-Carnicero, R. López-García, Optimal design of a hybrid ground source heat pump for an official building with thermal load imbalance and limited space for the ground heat exchanger, Renew. Energ. 195 (2022) 381–394.
[16] A. Behzadi, E. Gholamian, P. Ahmadi, A. Habibollahzade, M. Ashjaee, Energy, exergy and exergoeconomic (3E) analyses and multi-objective optimization of a solar and geothermal based integrated energy system, Appl. Therm. Eng. 143 (2018) 1011–1022.
[17] A. Habibollahzade, E. Houshfar, M. Ashjaee, K. Ekradi, Continuous power generation through a novel solar/geothermal chimney system: Technical/cost analyses and multi-objective particle swarm optimization, J. Clean Prod. 283 (2021) 124666.
[18] S.Z. Hu, Z. Yang, J. Li, Y.Y. Duan, Thermo-economic optimization of the hybrid geothermal-solar power system: A data-driven method based on lifetime off-design operation, Energy Convers. Manage. 229 (2021) 113738.
[19] G.F. Song, X.Z. Song, G.S. Li, R.N. Xu, W.J. Cao, C.R. Zhao, Multi-objective optimization of geothermal extraction from the enhanced geothermal system in Qiabuqia geothermal field, Gonghe Basin, Acta Geol. Sin.-Engl. 95 (6) (2021) 1844–1856.
[20] N. Wei, F. Yang, K.M. Lu, J.C. Xie, S.F. Zhang, A method of multi-objective optimization and multi-attribute decision-making for Huangjinxia reservoir, Appl. Sci. 12 (2022) 6300.
[21] Z.G. Zhang, X. Hu, Z.T. Liu, L.T. Zhao, Multi-attribute decision making: An innovative method based on the dynamic credibility of experts, Appl. Math. Comput. 393 (2021) 125816.
[22] J.C. Guo, P.W. Zhang, D. Wu, Z.J. Liu, X. Liu, S.C. Zhang, X.Y. Yang, H. Ge, Multi-objective optimization design and multi-attribute decision-making method of a distributed energy system based on nearly zero-energy community load forecasting, Energy 239 (2022) 122124.
[23] H. Yazdani, M. Baneshi, M. Yaghoubi, Techno-economic and environmental design of hybrid energy systems using multi-objective optimization and multi-criteria decision making methods, Energy Convers. Manage. 282 (2023) 116873.
[24] D.T. Nguyen, J.S. Chou, D.H. Tran, Integrating a novel multiple-objective FBI with BIM to determine tradeoff among resources in project scheduling, Knowl Based Syst 235 (2022) 107640.
[25] S. Breedveld, D. Craft, R. Van Haveren, B. Heijmen, Multi-criteria optimization and decision-making in radiotherapy, Eur. J. Oper. Res. 277 (2019) 1–19.
[26] G.S. Wang, X.Z. Song, Y. Shi, R. Zheng, J.C. Li, Z. Li, Production performance of a novel open loop geothermal system in a horizontal well, Energy Convers. Manage. 206 (2020) 112478.
[27] E.O. Holzbecher, Modeling Density-driven Flow in Porous Media: Principles, Numerics Software, Springer, New York, 1998.
[28] G.S. Wang, X.D. Ma, X.Z. Song, G.S. Li, Modeling flow and heat transfer of fractured reservoir: Implications for a multi-fracture enhanced geothermal system, J. Clean Prod. 365 (2022) 132708.
[29] Y. Shi, X.Z. Song, J.C. Li, G.S. Wang, R. Zheng, F.X. YuLong, Numerical investigation on heat extraction performance of a multilateral-well enhanced geothermal system with a discrete fracture network, Fuel 244 (2019) 207–226.
[30] P. Witherspoon, C. Amick, J. Gale, K. Iwai, Observations of a potential size effect in experimental determination of the hydraulic properties of fractures, Water Resour. Res. 15 (5) (1979) 1142–1146.
[31] D. Taler, Numerical modelling and experimental testing of heat exchangers, Springer International Publishing, Cham, Switzerland, 2019.
[32] Y. Shi, X.Z. Song, G.S. Wang, J.C. Li, L.D. Geng, X.J. Li, Numerical study on heat extraction performance of a multilateral-well enhanced geothermal system considering complex hydraulic and natural fractures, Renew Energ. 141 (2019) 950–963.
[33] W.C. Zhu, C.A. Tang, Micromechanical model for simulating the fracture process of rock, Rock. Mech. Rock. Eng. 37 (1) (2004) 25–56.
[34] W.C. Zhu, C.H. Wei, S. Li, J. Wei, M.S. Zhang, Numerical modeling on destress blasting in coal seam for enhancing gas drainage, Int. J. Rock Mech. Min. Sci. 59 (2013) 179–190.
[35] C.H. Wei, W.C. Zhu, Q.L. Yu, T. Xu, S. Jeon, Numerical simulation of excavation damaged zone under coupled thermal-mechanical conditions with varying mechanical parameters, Int. J. Rock Mech. Min. Sci. 75 (2015) 169–181.
[36] W.C. Zhu, C.H. Wei, Numerical simulation on mining-induced water inrushes related to geologic structures using a damage-based hydromechanical model, Environ. Earth Sci. 62 (2011) 43–54.
[37] Y. Shi, F.Q. Xu, X.Z. Song, G.S. Wang, Y.H. Zuo, X.J. Li, J.Y. Ji, Rock damage evolution in the production process of the enhanced geothermal systems considering thermal-hydrological-mechanical and damage (THM-D), Energy 285 (2023) 129421.
[38] W. Zhang, Z.L. Wang, T.K. Guo, C.G. Wang, F.M. Li, Z.Q. Qu, The enhanced geothermal system heat mining prediction based on fracture propagation simulation of thermo-hydro-mechanical-damage coupling: Insight from the integrated research of heat mining and supercritical CO_2 fracturing, Appl. Therm. Eng. 215 (2022) 118919.
[39] Q.H. Lei, N.G. Doonechaly, C.F. Tsang, Modelling fluid injection-induced fracture activation, damage growth, seismicity occurrence and connectivity change in naturally fractured rocks, Int. J. Rock Mech. Min. Sci. 138 (2021) 104598.
[40] Z.H. Lei, Y.J. Zhang, S.Q. Zhang, L. Fu, Z.J. Hu, Z.W. Yu, L.Z. Li, J. Zhou, Electricity generation from a three-horizontal-well enhanced geothermal system in the Qiabuqia geothermal field, China: Slickwater fracturing treatments for different reservoir scenarios, Renew Energ. 145 (2020) 65–83.
[41] X. Zhang, Z.Q. Huang, Q.H. Lei, J. Yao, L. Gong, Z.X. Sun, W.D. Yang, X. Yan, Y. Li, Impact of fracture shear dilation on long-term heat extraction in Enhanced Geothermal Systems: Insights from a fully-coupled thermo-hydro-mechanical simulation, Geothermics 96 (2021) 102216.
[42] Z.Q. Qu, W. Zhang, T.K. Guo, Influence of different fracture morphology on heat mining performance of enhanced geothermal systems based on COMSOL, Int. J. Hydrog. Energy 42 (29) (2017) 18263–18278.
[43] Q. Cui, Y. Shi, Y. Zhang, R. Wu, Y. Jiao, Comparative study on the thermal performance and economic efficiency of vertical and horizontal ground heat exchangers, Adv. Geo-Energy Res. 7 (1) (2023) 7–19.
[44] Y. Kong, Z. Pang, H. Shao, O. Kolditz, Optimization of well-doublet placement in geothermal reservoirs using numerical simulation and economic analysis, Environ. Earth Sci. 76 (3) (2017) 118.
[45] K. Deb, A. Pratap, S. Agarwal, T. Meyarivan, A fast and elitist multiobjective genetic algorithm: NSGA-II, IEEE Trans. Evol. Comput. 6 (2) (2002) 182–197.
[46] Q.F. Zhang, H. Li, MOEA/D: A multiobjective evolutionary algorithm based on decomposition, IEEE Trans. Evol. Comput. 11 (6) (2007) 712–731.
[47] C.A. Coello Coello, M.S. Lechuga, MOPSO: A proposal for multiple objective particle swarm optimization, In Proceedings of the 2002 Congress on Evolutionary Computation, CEC'02 (Cat. No.02TH8600), IEEE, Honolulu, 1051-1056.
[48] R. Cheng, Y.C. Jin, M. Olhofer, B. Sendhof, A reference vector guided evolutionary algorithm for many-objective optimization, IEEE Trans. Evol. Comput. 20 (5) (2016) 773–791.
[49] Y. Tian, R. Cheng, X.Y. Zhang, Y.C. Jin, PlatEMO: A MATLAB platform for evolutionary multi-objective optimization [educational forum], IEEE Comput. Intell. Mag. 12 (4) (2017) 73–87.
[50] D.A. Van Veldhuizen, Multiobjective evolutionary algorithms: classifications, analyses, and new innovations, Graduate School of Engineering, Air Force Institute of Technology, Wright-Patterson AFB, Ohio, USA, 1999. Ph.D. Thesis.
[51] J. Bader, E. Zitzler, HypE: An algorithm for fast hypervolume-based many-objective optimization, Evol Comput. 19 (1) (2011) 45–76.
[52] C.A.C. Coello, M. Reyes Sierra, A study of the parallelization of a coevolutionary multi-objective evolutionary algorithm. In: Monroy, R., Arroyo-Figueroa, G., Sucar, L.E., Sossa, H. (eds.) MICAI 2004. LNCS (LNAI), 2972, 688–697. Springer, Heidelberg.
[53] J.R. Schott, Fault tolerant design using single and multicriteria genetic algorithm optimization, Master's Thesis, Air Force Institute of Technology, Wright-Partterson AFB OH, Ohio, USA, 1995.
[54] T.L. Saaty, The Analytic Hierarchy Process, McGraw-Hill, New York, 1980.
[55] P.F. Krstanovic, V.P. Singh, Evaluation of rainfall networks using entropy: I. Theoretical development, Water Resour. Manag. 6 (1992) 279-293.
[56] C.L. Hwang, K.S. Yoon, Multiple attribute decision making: methods and applications, Springer-Verlag, Berlin, 1981.
[57] S. Opricovic, Multicriteria optimization of civil engineering systems, Ph.D. Thesis, Faculty of Civil Engineering, Belgrade, SRB, 1998.